Sensor and Simulation Notes

Note 354

January 1993

Optimizing the Feed Impedance of Impulse Radiating Antennas
Part I: Reflector IRAs

Everett G. Farr
Farr Research
614 Paseo Del Mar NE
Albuquerque, NM 87123

Abstract

When designing a reflector Impulse Radiating Antenna, one must choose an appropriate feed impedance. Using the simplest approximations valid for high feed impedances, one finds that lower feed impedances are always preferable. However, low feed impedances imply thick feed arms, which increase feed blockage for many designs, thus reducing the radiated field. Low feed impedances also lead to a breakdown of the approximation that the effective aperture height is equal to the radius of an aperture for circular apertures. Thus, even when there is no feed blockage, there is a reduced aperture height at low feed impedances.

We calculate here the radiated field based on a contour integration technique that takes into account feed blockage. With these calculations, one can find the optimal feed impedance for a given configuration of feed arms. The analysis is valid in the limit of fast risetimes, and is carried out for three different feed structures.

I. Introduction

Simple models of reflector-type Impulse Radiating Antennas (IRAs) have to date ignored feed blockage [1, 2]. Under these simple models, one finds simply that a low feed impedance is always preferable to a higher one. However, lower feed impedances contribute more to aperture blockage, which reduces the radiated field. Even without feed blockage, the simple model is known to break down at low impedances. Clearly, the simple model needs to be extended to include aperture blockage and the effects of lower impedance. This is accomplished by using a contour integration technique similar to that used in [3], while taking into account feed blockage, and including additional terms in the contour integration.

By way of review, consider the IRA of Figure 1.1, with diameter D, focal distance F, and feed impedance $Z_c=Z_o/f_g$. Our simple model leads to a far field on boresight of

$$E_y(r,t)=\frac{V_o}{r}\frac{D}{4\pi c f_g}\left[\delta_a(t-2F/c)\ -\ \frac{c}{2F}\left[u(t)-u(t-2F/c\right]\right] \tag{1.1}$$

where the driving voltage across the feed arms is a step function, $V(t)=V_o\,u(t)$ and $\delta_a(t)$ is the approximate delta function [3]. If we now keep power constant, the radiated field is proportional to $f_g^{-1/2}$. If we choose to keep voltage constant, the radiated is proportional to $1/f_g$. In either case, these simple models suggest a small f_g is always preferable. This would imply, however, a large aperture blockage, so we must find a way to compromise.

This paper builds on the work of Y. Rahmat-Samii and D. V. Giri in [4, 5]. These papers calculated the feed blockage as a function of frequency and angle from boresight for the configuration of facing plate feeds at 400 Ω impedance. In this paper, we calculate the high-frequency limit of the radiated field on boresight for configurations with arbitrary feed impedances, and with a variety of feed geometries. Furthermore, we show how to apply these results to choosing the optimal feed impedance under a variety of conditions. The techniques of [5] could be used to optimize the feed impedance, however, it seems more convenient to use the techniques developed here.

We begin by defining the terms necessary for a description of the radiated field. These are essentially extensions of the definition of transient gain as described in [6]. Having defined these gains, we then calculate them for a number of different feed geometries, building upon the contour integration methods of [3]. We handle both two-arm and four-arm configurations of circular cones, curved plates, and coplanar plate conical feeds.

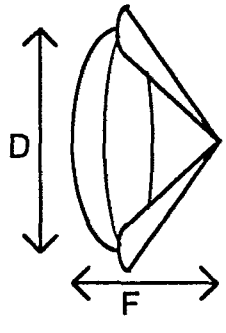

Figure 1.1. An Impulse Radiating Antenna.

This is the first part of an anticipated two-part series. A later paper will deal with optimizing the feed impedance of very long TEM horns, or TEM horns with a lens in the aperture (reflector IRAs).

II. Gain Definitions

In this section we identify the problem to be solved, and we specify gain definitions that describe the output of the antenna. Consider Figure 2.1, which shows an IRA, constructed of a paraboloidal reflector of circular cross section, fed by a conical TEM transmission line. When excited by a step-function voltage, it has been shown that the field in some aperture plane in front of the paraboloid is described by the two dimensional problem of two wires [1, App. A]. This two-dimensional problem is just the stereographic projection of the conical geometry onto an aperture plane [1]. We review here how to calculate the radiated field, and we also specify how to express the gain of such an arrangement.

The aperture electric field is described by the field of a quasistatic transmission line that is turned on suddenly. In other words, the electric field is expressed as

$$\vec{E}^{ap}(x',y',t) = E(x',y')\,u(t) \tag{2.1}$$

It was shown in [3] that the aperture field $E(x',y')$ can be expressed as the gradient of a complex potential,

$$E(x',y') = E(z) = E_x - j\,E_y = -\frac{V}{\Delta u}\frac{dw(z)}{dz} \tag{2.2}$$

where

$$z = x + j\,y, \quad w(z) = u(z) + j\,v(z), \qquad f_g = \Delta u / \Delta v \tag{2.3}$$

In this formulation, Δv is the change in v around one of the conductors, and Δu is the difference in u from one conductor to the other. In was also shown in [3] that the radiated field on boresight is

$$\vec{E}^{rad}(r,t) = \frac{V}{r}\frac{h_a}{2\pi c\, f_g}\,\delta_a(t - r/c) \tag{2.4}$$

where

$$h_a = -\frac{f_g}{V}\iint_{S_a} E_y(x',y')\,dx\,dy = -\frac{1}{\Delta v}\oint_{C_a} v(y)\,dy \tag{2.5}$$

In the above equation, S_a is the portion of the aperture that is not blocked by the feed, and C_a is the contour around this aperture. All contour integrals in this paper are in the counterclockwise direction. In [3] an approximation was made that feed blockage could be ignored, in which case the integral is trivial to calculate as ~$D/2$, for high impedances. This led to the radiated field of (1.1). A more accurate integral, however, excludes the portion of the aperture integral that is blocked by the feed. The remainder of this paper will be dedicated to calculating the above integral for a number of configurations. But before doing that, we need to specify how to express the final results.

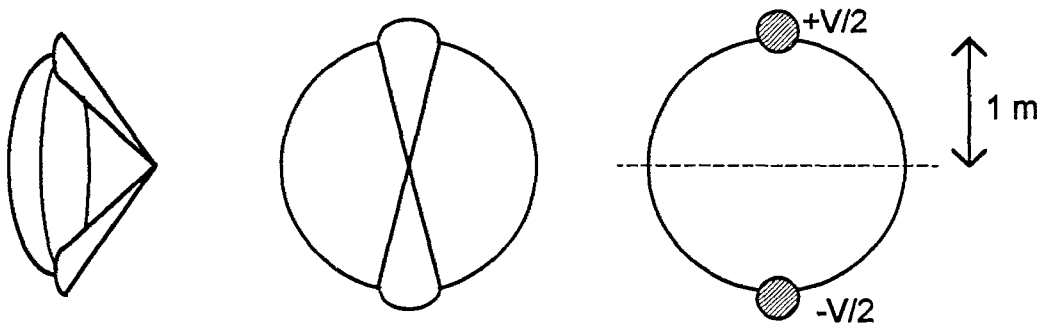

Figure 2.1. A two-arm IRA configuration (left and center), and the stereographic projection of the conical arms into the aperture plane (right).

Let us now consider how to express the gain of such an antenna. We wish to optimize the feed impedance under two distinct conditions -- constant input power, and constant input voltage. Thus, we need two definitions of gain that, when optimized, provide the optimal feed impedance under two distinct conditions. In order to express these parameters, let us recall the definition of gain as given in [6]

$$G_p = 2\pi c\sqrt{f_g}\,\frac{\left\| r\,\vec{E}^{rad}(r,t)\right\|}{\left\|\dfrac{dV^{inc}(t)}{dt}\right\|} \tag{2.6}$$

Recall that this definition is a function of the shape of the driving voltage and the choice of the norm. Since we are now going to drive our antenna with a step function in transmission, let us assume a waveshape of a step function. Furthermore, a sensible choice for the norm is the area of the resulting delta function, the so-called A-norm of [6]. Substituting (2.4) into (2.6), and recognizing that $V^{inc}(t) = V\,u(t)$, we find

$$G_p = \frac{h_a}{\sqrt{f_g}} \tag{2.7}$$

In this equation the subscript p indicates a gain that is normalized to power. By this we mean that if the square root of the input power ($Vf_g^{-1/2}$) is held constant in (2.4), then the radiated field is proportional to $h_a f_g^{-1/2}$. We will refer to this as the power-normalized gain. Note that the units of this gain are meters, which is typical of gain definitions in the time domain [6].

Next, we extend this concept of gain to the case where input voltage is held constant. This has a practical application where an antenna feed can sustain some maximum voltage, due to voltage breakdown. For this case, we modify (2.6) by removing the geometric factor f_g, to find

$$G_v = 2\pi c \frac{\left\| r\,\vec{E}^{rad}(r,t) \right\|}{\left\| \frac{dV^{inc}(t)}{dt} \right\|} \tag{2.8}$$

Now, the subscript v indicates that the gain is normalized to a constant input voltage. Substituting the radiated field (2.4) into the above equation gives

$$G_v = \frac{h_a}{f_g} \tag{2.9}$$

This is the quantity one must optimize to get the best radiated field when the voltage is kept constant. Again, one can check this by noting in (2.4) that if the input voltage is held constant, the radiated field is proportional to h_a/f_g. We will refer to this as the voltage-normalized gain. As before, the units of this gain are meters.

Note that in [6] care was taken to confine gain definitions to power-based, or power-normalized definitions. This was done in order to be consistent with IEEE gain definitions in the frequency (CW) domain. It is clear, however, that under certain circumstances a voltage-based gain makes more sense. We therefore should allow the flexibility to define the gain that is most useful to a particular problem.

Thus, we see that in order to optimize the radiated field under conditions of constant input power, one optimizes the power-normalized gain, $G_p=h_a/f_g^{1/2}$, with respect to feed impedance. Furthermore, if one wishes to optimize radiated field for a constant input voltage, one optimizes the voltage-based gain, $G_v=h_a/f_g$, with respect to feed impedance.

Finally, we consider the case of an IRA fed by four arms (Figure 2.2). We calculate the radiated field for an excitation of just two arms at a time. Although one would normally excite all four arms at once, it is simplest to treat two arms at a time, and then take the linear superposition of each pair of arms later. To find the radiated fields, we calculate a new effective height of the aperture, similar to (2.5), except that we exclude the portion of the integral due to the second pair of feed arms. If we call the new aperture height h_{a4}, then our two gains are

$$G_{p4} = \frac{h_{a4}}{\sqrt{f_g}}, \qquad G_{v4} = \frac{h_{a4}}{f_g} \tag{2.10}$$

Let us now apply these gains to some typical examples.

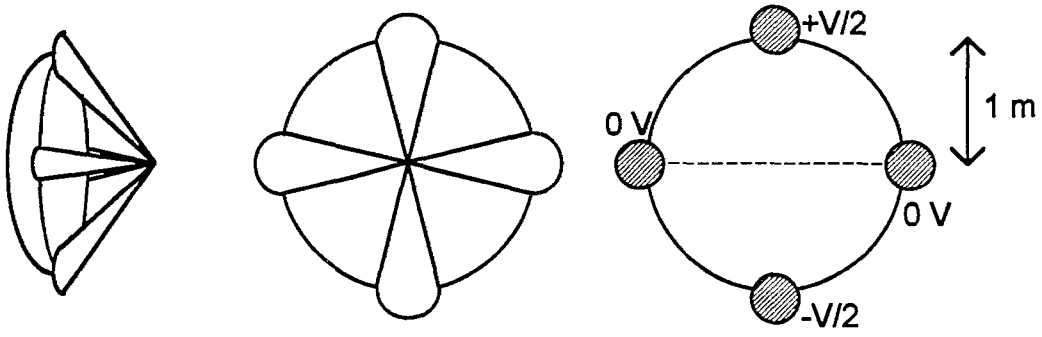

Figure 2.2 A four-arm IRA configuration (left and center), and its stereographic projection into the aperture plane (right).

III. Circular Cone Feeds

Consider now perhaps the simplest case one can think of, that of two circular cone feeds shown in Figure 2.1. The contour one must integrate around is shown in Figure 3.1. For our purposes, it is simplest to keep b_e, the electrical center of the wire, equal to one meter, and to calculate all our gains for a reflector of radius 1 m. Note that

$$b^2 = b_e^2 + a^2 \tag{3.1}$$

or if we assume $b_e = 1$ m,

$$b^2 = 1 + a^2 \tag{3.2}$$

We have chosen to work in unitless dimensions, adding them at the end. If we do not do this, then we have to carry the symbol b_e through all of our calculations, which is somewhat cumbersome.

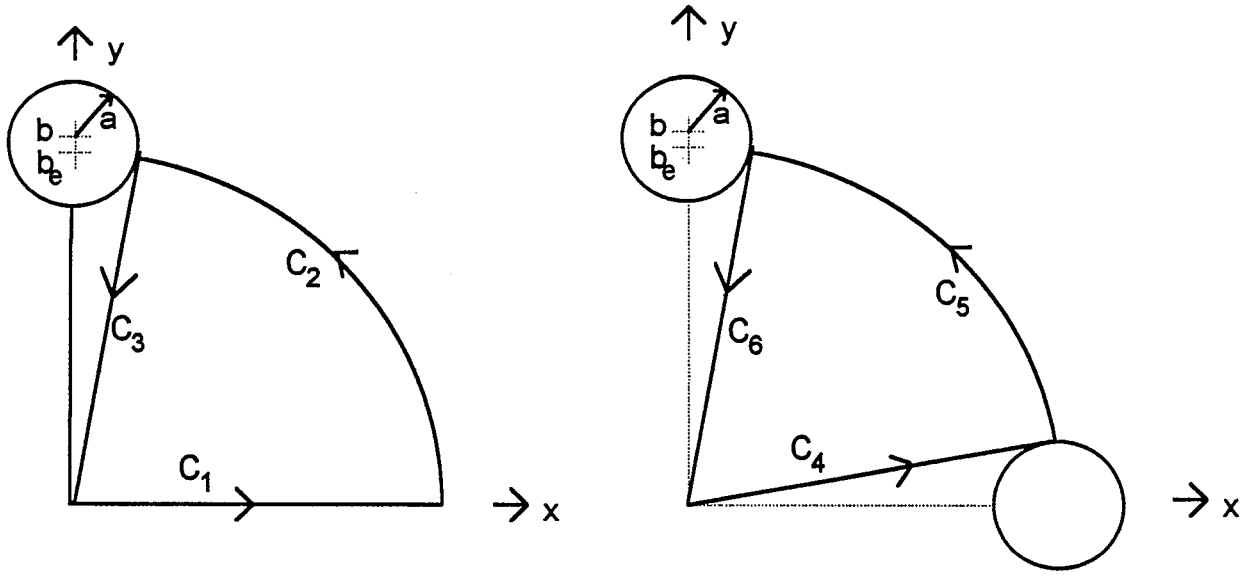

Figure 3.1. Integration contour for two round wires (left) and four round wires (right).

We now need to calculate the aperture height h_a as a function of impedance using (2.5). To do so, we need the complex potential function describing this geometry. According to [7, 3], the potential function is

$$w = u(z) + j\,v(z) = 2\,j\,\mathrm{arccot}(z) = \ln\left(\frac{z+j}{z-j}\right) \tag{3.3}$$

A map of this potential function is plotted in Figure 3.2, which is reproduced from [3]. This can be separated into

$$\begin{aligned} u(z) &= \frac{1}{2}\ln\left[\frac{x^2+(1+y)^2}{x^2+(1-y)^2}\right] \\ v(z) &= \arctan\left[\frac{2x}{x^2+y^2-1}\right] \end{aligned} \tag{3.4}$$

Alternatively, one could express the above as

$$\begin{aligned} x &= \frac{\sin(v)}{\cosh(u)-\cos(v)} \\ y &= \frac{\sinh(u)}{\cosh(u)-\cos(v)} \end{aligned} \tag{3.5}$$

The conductors are defined by circles of $\pm u_o$, so the feed impedance is

$$f_g = \frac{\Delta u}{\Delta v} = \frac{2u_o}{2\pi} = \frac{u_o}{\pi} = \frac{1}{\pi}\,\mathrm{arccosh}(b/a) \tag{3.6}$$

The aperture height from (2.5) is now just

$$h_a = -\frac{4}{\Delta v}\oint_{C_a'} v(y)\,dy \tag{3.7}$$

where C_a' is the contour around the exposed portion of the aperture in the upper right quadrant. Furthermore, for this configuration $\Delta v = 2\pi$.

Next, let us calculate where the edge of the reflector intersects with the wire at the top. The top wire is defined by a circle of constant $u = u_o$, which is expressed as

$$x^2 + \left[y - \coth(u_o)\right]^2 = \mathrm{csch}^2(u_o) \tag{3.8}$$

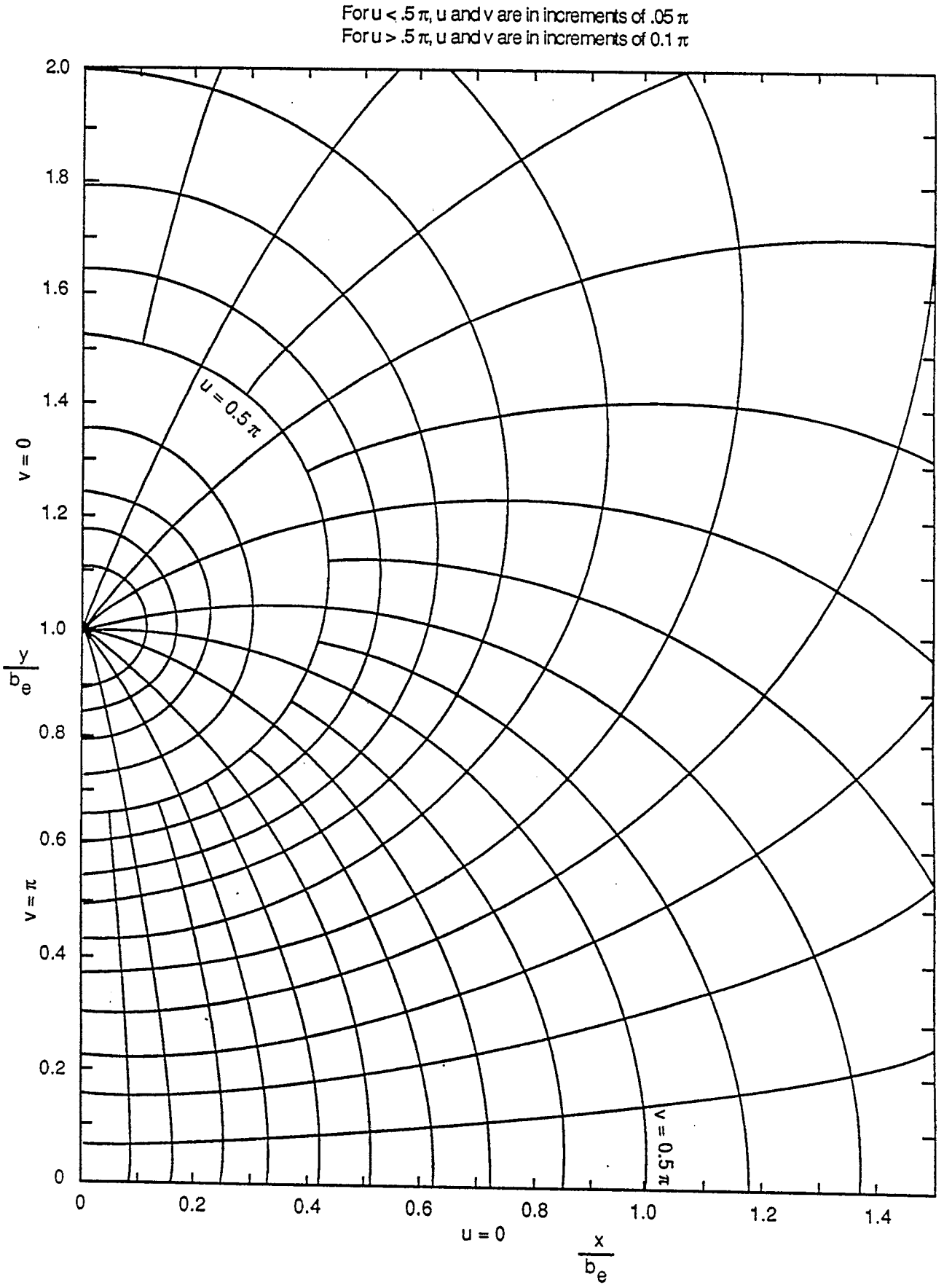

Figure 3.2. Complex potential for two wires, upper right quadrant.

Furthermore, the edge of the reflector is defined by

$$x^2 + y^2 = 1 \tag{3.9}$$

Combining the above two equations, we find the intersection of the upper conductor with the rim of the reflector occurs at

$$(x_o, y_o) = \left(\operatorname{sech}(u_o),\ \tanh(u_o) \right) \tag{3.10}$$

Furthermore, we need for the four-arm case the intersection of the edge of the reflector with the wire on the right. By symmetry, this occurs simply at

$$(x_1, y_1) = \left(\tanh(u_o),\ \operatorname{sech}(u_o) \right) \tag{3.11}$$

We now have enough information to calculate the contour integral in (3.7).

Consider first the contour integral for the two-arm case. On the horizontal arm of the contour C_1, $dy = 0$, so there is no contribution due to it. Thus,

$$I_1 = \int_{C_1} v(y)\, dy = 0 \tag{3.12}$$

Along the outer edge of the reflector, C_2, $v = \pi/2$, so

$$I_2 = \int_{C_2} v(y)\, dy = \frac{\pi}{2} \tanh(u_o) \tag{3.13}$$

On C_3, $x = y \operatorname{csch}(u_o)$, so

$$v(y) = \pi + \arctan\left[\frac{2\, y \operatorname{csch}(u_o)}{\left[y \coth(u_o) \right]^2 - 1} \right] \tag{3.14}$$

Note that we have added π to the result, in order to use the correct branch of the arctangent function. Thus, the integral along the radial portion becomes

$$I_3 = \int_{C_3} v(y)\, dy = \int_{\tanh(u_o)}^{0} \left[\pi + \arctan\left[\frac{2\, y \operatorname{csch}(u_o)}{\left[y \coth(u_o) \right]^2 - 1} \right] \right] dy \tag{3.15}$$

With these integrals defined, we find the overall aperture height from (3.7) as simply

$$h_a = -\frac{2}{\pi}(I_1 + I_2 + I_3) \tag{3.16}$$

This completes the formulation for the two-arm case. The various integrals are carried out numerically using the program *Mathematica* [12]. In the case shown here, this program is merely a convenience. However, for the more complicated cases to follow, this program is used as an implementation of special functions with complex arguments.

Next, we consider the four-arm case. Along the bottom portion of the contour, we have $x = y\sinh(u_o)$. Substituting into (3.4) gives

$$v(y) = \pi + \arctan\left[\frac{2y\sinh(u_o)}{[y\cosh(u_o)]^2 - 1}\right] \tag{3.17}$$

so the contour integral along I_4 is

$$I_4 = \int_{C_4} v(y)\,dy = \int_0^{\operatorname{sech}(u_o)} \left[\pi + \arctan\left[\frac{2y\sinh(u_o)}{[y\cosh(u_o)]^2 - 1}\right]\right] dy \tag{3.18}$$

Next, the portion of the contour integral along the arc, C_5, is simply

$$I_5 = \oint_{C_5} v(y)\,dy = \frac{\pi}{2}\left[\tanh(u_o) - \operatorname{sech}(u_o)\right] \tag{3.19}$$

Finally, along C_6, the integral is the same as for the two-arm case. Thus,

$$I_6 = I_3 \tag{3.20}$$

and the overall aperture height for the four-arm case is

$$h_{a4} = -\frac{2}{\pi}(I_4 + I_5 + I_6) \tag{3.21}$$

This completes the formulation of the four-arm case.

Before plotting our results, we need to establish a value for Z_o, the impedance of free space. We have the option of expressing our results as a function of feed impedance, in Ohms, or in terms of the normalized feed impedance, f_g, which is unitless. We choose to use actual impedance, however, we must be careful to specify the impedance of free space Z_o as accurately as possible. Thus, we specify

$$Z_o = \mu_o c = 4\pi\times 10^{-7}\ \mathrm{H/m} \times 2.99790\times 10^{8}\ \mathrm{m/s} = 376.727\,\Omega \tag{3.22}$$

This provides sufficient accuracy, since we claim no more than four significant figures of accuracy in our numerical results.

Let us present now our results. First, we calculate the feed impedance as a function of a/b and a/b_e (Figure 3.3). These results help to specify the geometry, since all future results are plotted as a function of feed impedance.

Next, we calculate the aperture height as a function of characteristic impedance, for both the two-arm and four-arm cases (Figure 3.4). Recall that all of these results are presented for the case of an aperture radius of 1 m ($b_e = 1$ m). For these cases, when we ignore aperture blockage, we expect the aperture height to be 1 m [3], and that is what we see in the limit of high impedances. Note that the penalty for the second pair of arms is small at high impedances, and more substantial at smaller impedances.

Next we plot the power-normalized gain, $h_a/f_g^{1/2}$, as a function of feed impedance (Figure 3.5). This is the quantity one optimizes when a fixed amount of power is available. Although the maximum is rather broad, we can see a peak. We find the peak for the two-arm case to be at $Z_c = 311.9\ \Omega$, where $G_p = 0.8491$ m. For the four-arm case, the peak occurs at $Z_c = 406.2\ \Omega$, where $G_{p4} = 0.8060$ m. The second pair of arms pushes the optimal case to higher impedances (thinner feed arms) where there is less aperture blockage, as we expect.

Finally, we calculate the voltage-normalized gain, h_a/f_g, for both the two-arm and four-arm cases (Figure 3.6). This is the quantity one optimizes when a fixed maximum voltage is available. For the two-arm case, we find that the optimal value occurs at $Z_c = 0$. Since one cannot have an impedance of zero, in practice one chooses to make the feed arms as large as possible within the space available. The four-arm case is also shown in Figure 3.6, having a maximum at 266.8 Ω, where $G_{v4} = 0.8688$ m.

Note that in the four-arm case we cannot calculate the various gains to as low an impedance as we might like, since we are not modifying the impedance calculation to account for the second pair of arms. As long as the second pair of arms is thin, this is similar to placing a conductor in the plane of symmetry, which has no effect. As the second pair of arms becomes thicker at lower impedances, the approximation breaks down.

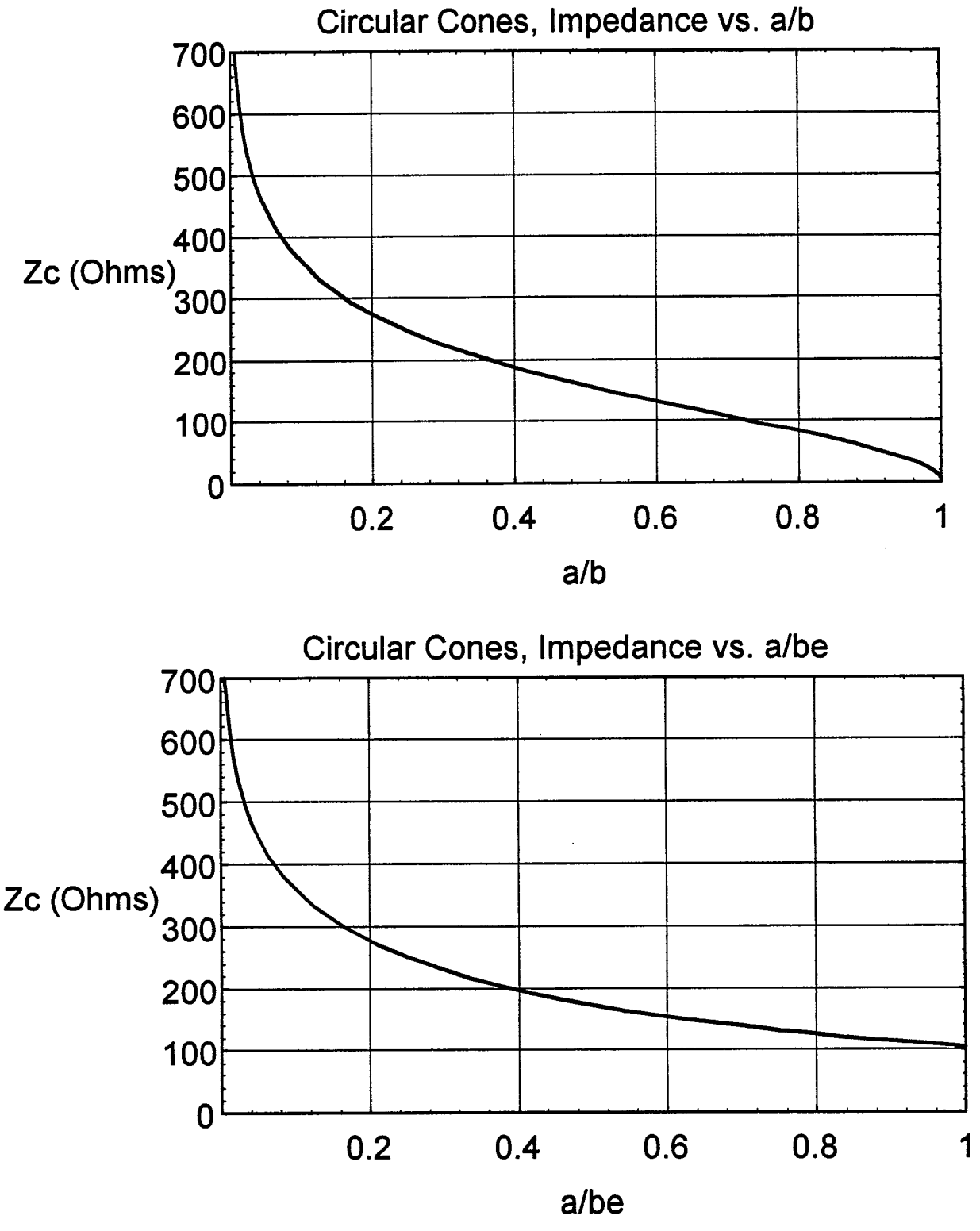

Figure 3.3. Feed impedance as a function of wire radius.

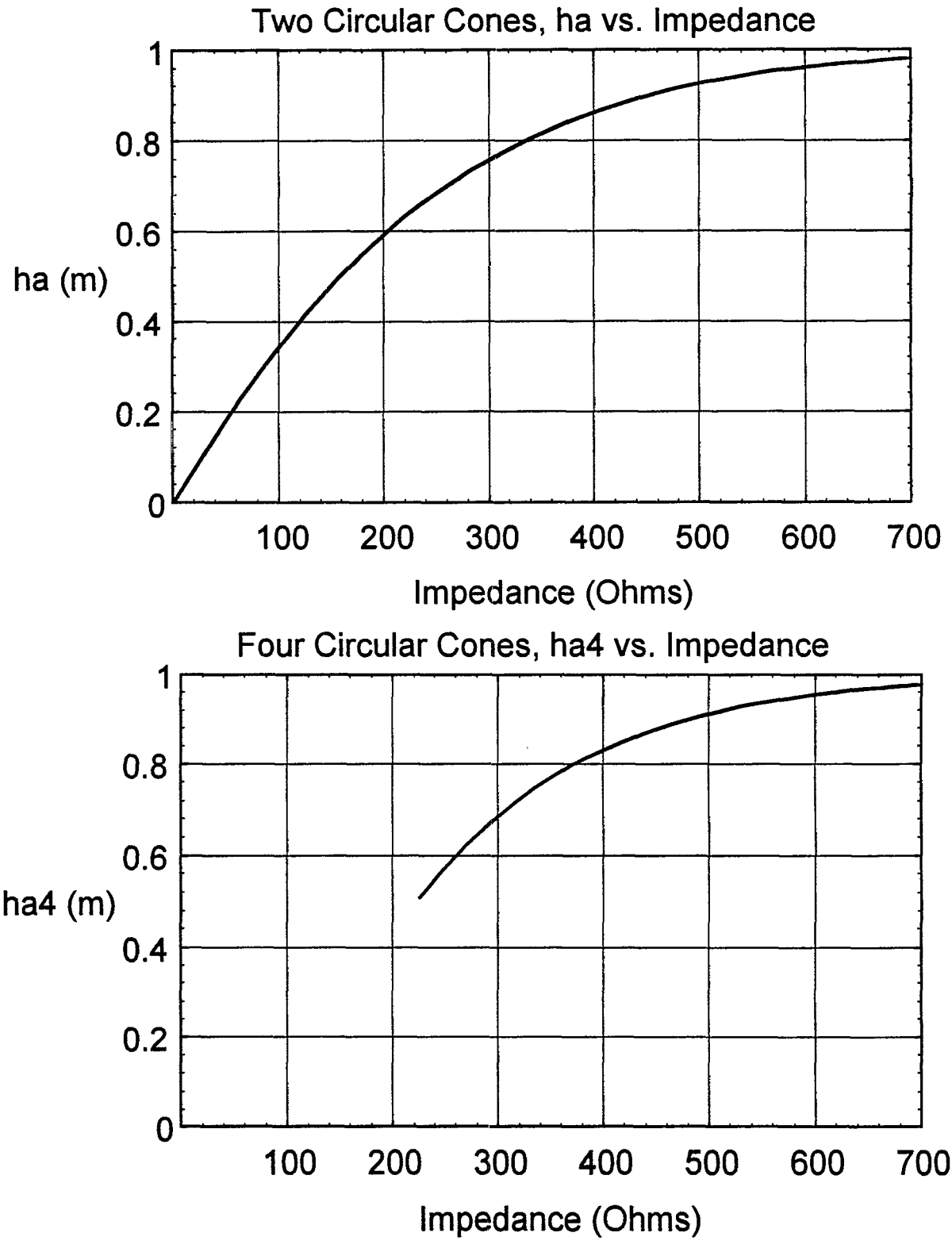

Figure 3.4. Variation of aperture height with feed impedance for two-arm (top) and four-arm (bottom) circular cone feeds.

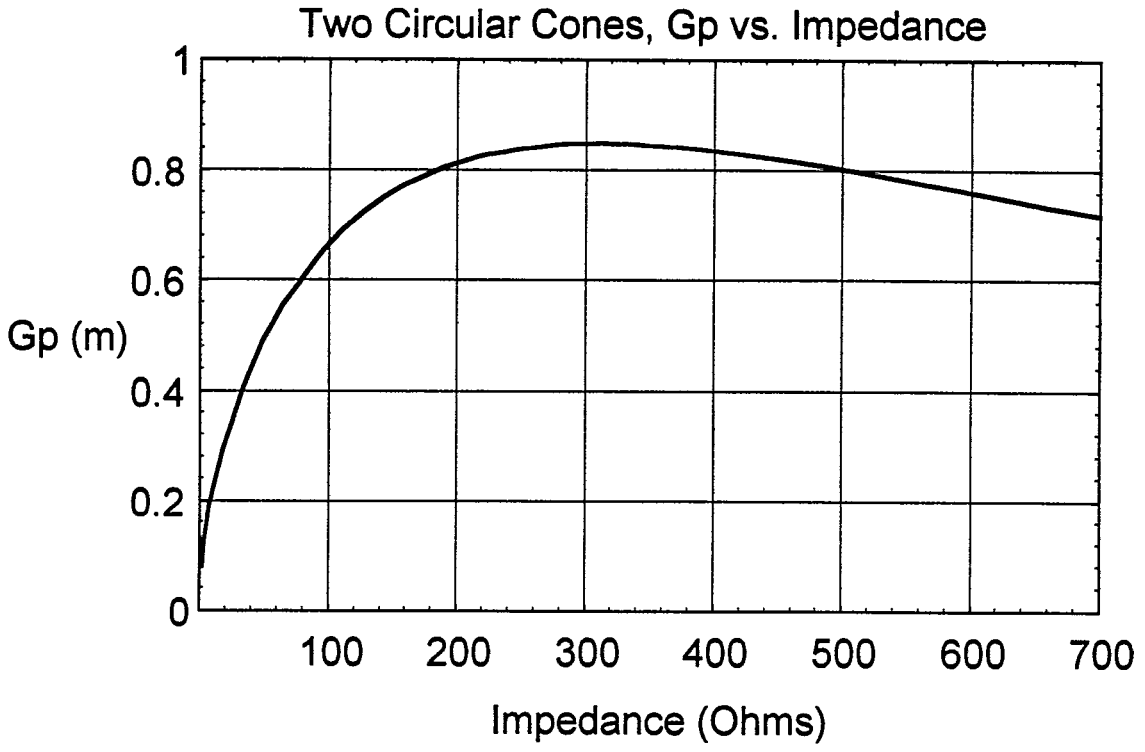

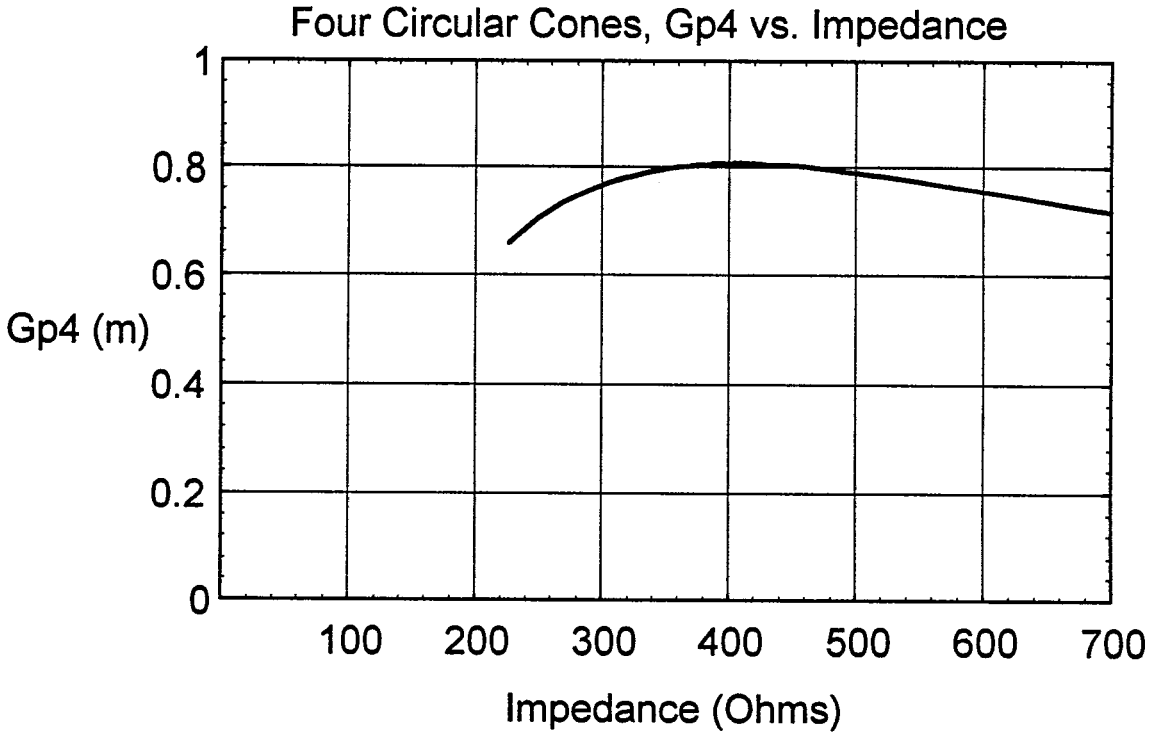

Figure 3.5. Variation of power-normalized gain with feed impedance, for circular cone feeds. The two-arm case (top) has a peak of $G_p = 0.8491$ m for $Z_c = 311.9\ \Omega$. The four-arm case (bottom) has a peak of $G_{p4} = 0.8060$ m for $Z_c = 406.2\ \Omega$.

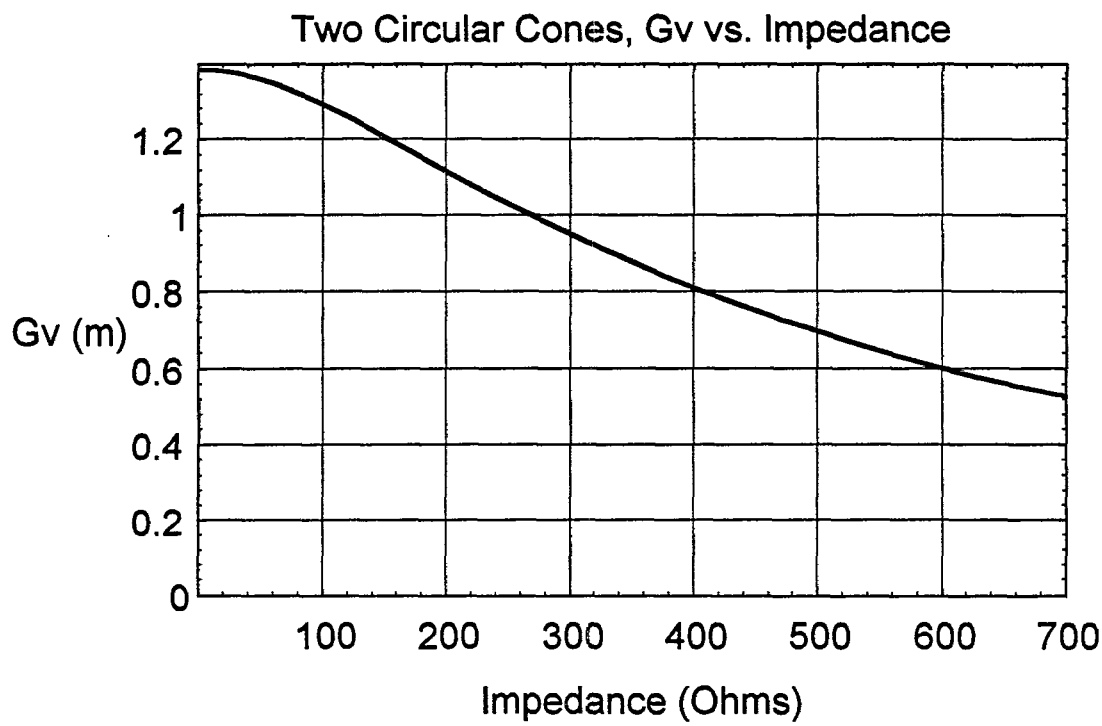

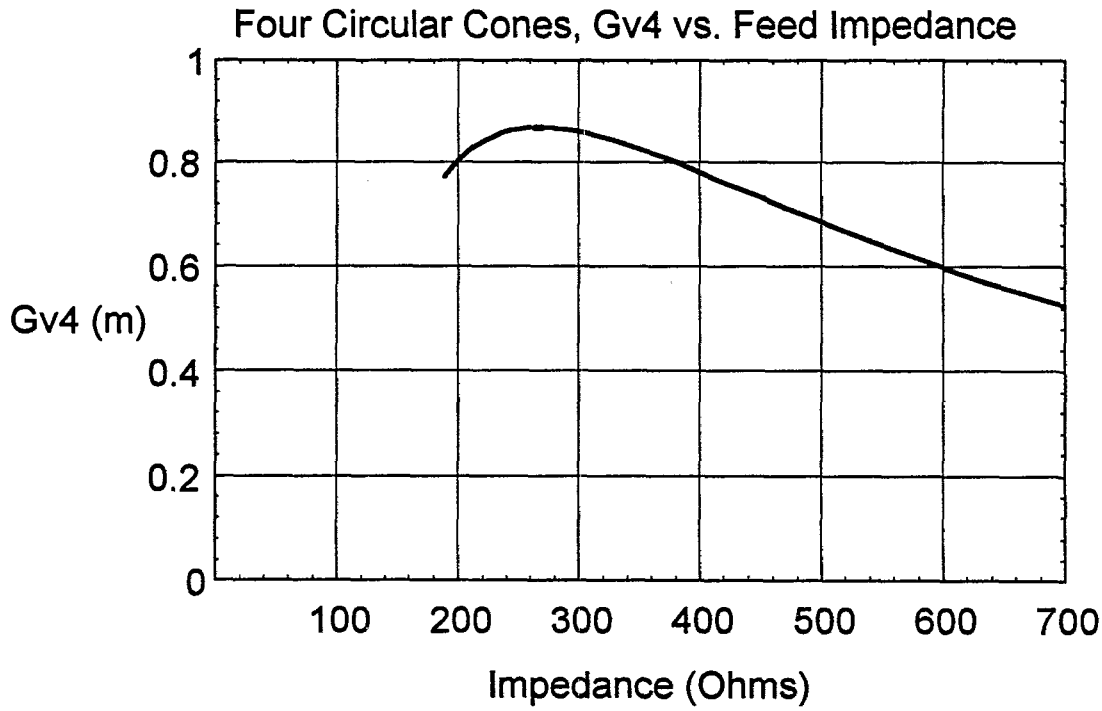

Figure 3.6. Variation of voltage-normalized gain with feed impedance, for the two-arm and four-arm circular cone feeds. The four-arm case (bottom) has a peak of $G_{v4} = 0.8688$ m for $Z_c = 266.8\ \Omega$.

V. Curved Plates

Next, we consider the case of curved plates that are confined to lie in a circle of radius 1 m. The projection of this geometry into the aperture plane is shown in Figure 4.1. The procedure for solving this is exactly the same as that for the circular cones, treated in the previous section.

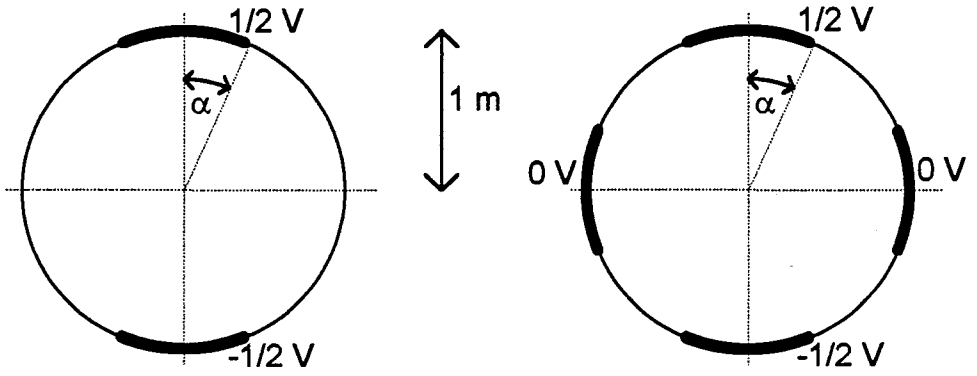

Figure 4.1. The geometry for curved plates, two-arm and four-arm configurations.

According to [8, 11], the potential function is described by

$$w = \operatorname{arcsn}\left[\frac{1}{j\,m^{1/4}}\frac{z-1}{z+1}\right], \qquad z = \frac{1+j\,m^{1/4}\operatorname{sn}(w|m)}{1-j\,m^{1/4}\operatorname{sn}(w|m)} \tag{4.1}$$

where sn($w|m$) is one of the Jacobian elliptic functions [9], and arcsn is its inverse. This complex potential function is plotted in Figure 4.2, which is reproduced from [8]. The relationship between m and α is

$$\tan(\alpha) = \frac{1-m^{1/2}}{2\,m^{1/4}}, \qquad m = \left[\frac{1-\sin(\alpha)}{\cos(\alpha)}\right]^4 \tag{4.2}$$

The characteristic impedance of the configuration is $Z_c = Z_o f_g$, where

$$f_g = \frac{K(m)}{K(m_1)} \tag{4.3}$$

In this equation, $K(m)$ is the complete elliptic integral [9], and $m_1 = 1 - m$.

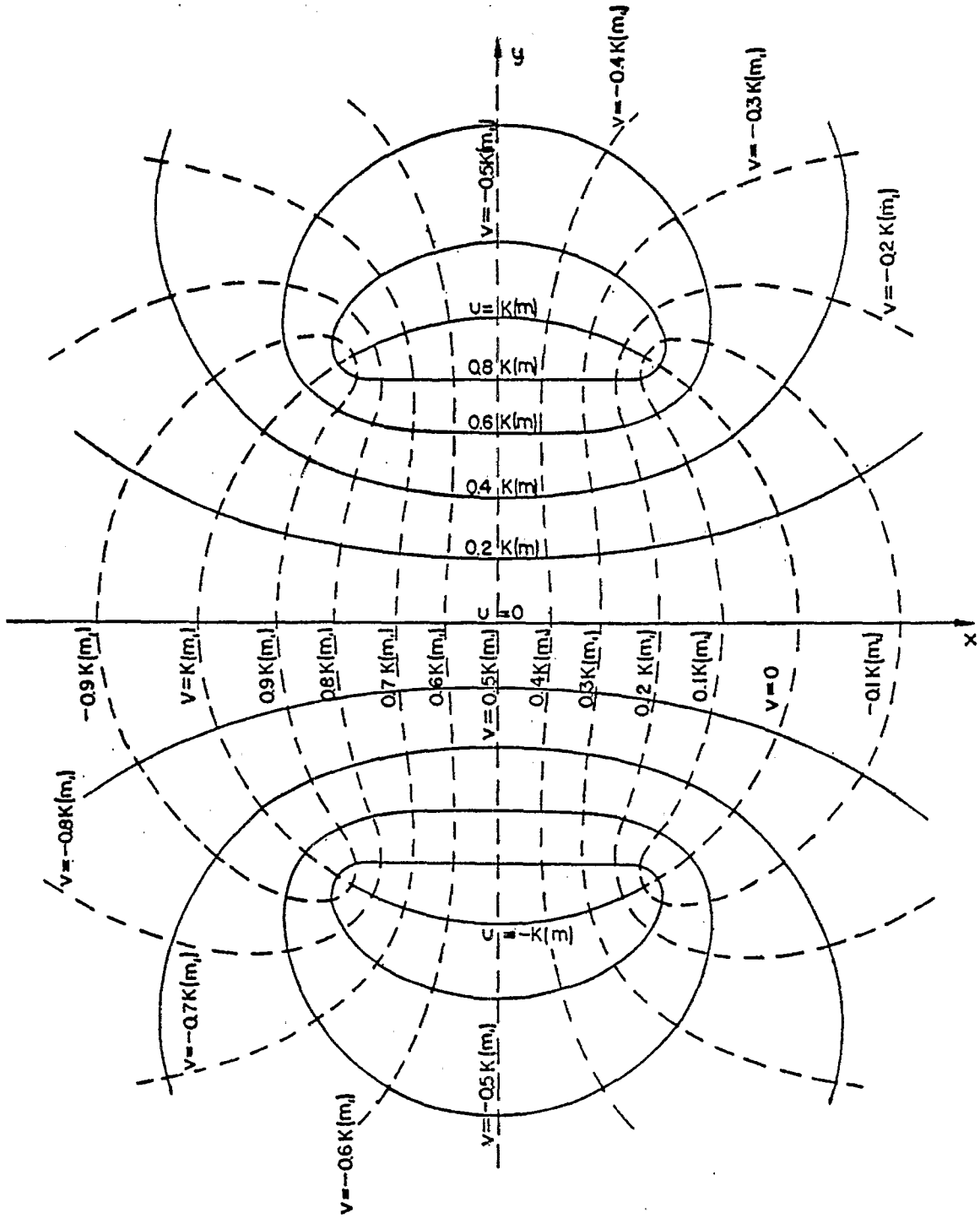

Figure 4.2. Complex potential for curved plates.

We now need to find the aperture height. As with the circular cones,

$$h_a = -\frac{4}{\Delta v} \oint_{C'_a} v(y)\, dy \tag{4.4}$$

where $v(y) = \mathrm{Im}[w(y)]$, and the contour C'_a is the contour that surrounds the portion of the aperture in the upper right quadrant that is not blocked by the feed arms. These contours are shown for both the 2-arm and 4-arm cases in Figure 4.3. Furthermore, $\Delta v = 2K(m_1)$ for this configuration.

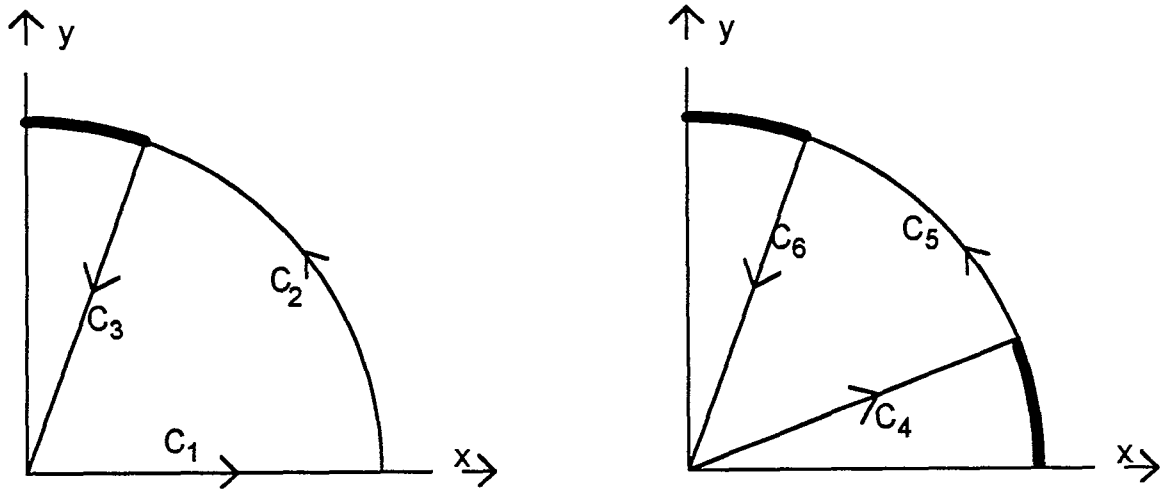

Figure 4.3. The integration contours for the 2-arm and 4-arm curved plate feeds.

We begin with the two-arm case. Along C_1, $dy = 0$, so $I_1 = 0$. It was shown in [8] that along the circular arc C_2, $v(y) = 0$, so $I_2 = 0$. Thus, the only contour of interest is C_3. Along this contour, $x = y \tan(\alpha)$, so

$$I_3 = \int_{C_3} v(y)\, dy = \int_{\cos(\alpha)}^{0} \mathrm{Im}\left[w\left(y\tan(\alpha) + j\, y\right)\right] dy \tag{4.5}$$

where $w(z)$ is defined in (4.1). Thus, the aperture height, from (4.4), is

$$h_a = -\frac{2}{K(m_1)} I_3 \tag{4.6}$$

This concludes the formulation of the two-arm case.

Let us consider now the four-arm case. Along C_4, $x = y \cot(\alpha)$, so

$$I_4 = \int_{C_4} v(y)\,dy = \int_0^{\sin(\alpha)} \mathrm{Im}\left[w\left(y\cot(\alpha) + j\,y\right)\right] dy \tag{4.7}$$

Furthermore, along C_5 $v(y) = 0$, so $I_5 = 0$. In addition, along C_6 we get the same result as for C_3, so

$$\begin{aligned} I_5 &= 0 \\ I_6 &= I_3 \end{aligned} \tag{4.8}$$

Thus, the aperture height for the four-arm case is just

$$h_{a4} = -\frac{2}{K(m_1)}\left[I_4 + I_6\right] \tag{4.9}$$

This completes the formulation for the four-arm configuration.

We begin our results by plotting the feed impedance as a function of α (Figure 4.4). We do so because all subsequent results will be expressed in terms of the feed impedance.

Next, we calculate the aperture heights for the two-arm and four-arm cases (Figure 4.5). All calculations, as before, are for an aperture of radius 1 m. Thus, when one ignores aperture blockage at high impedances, one calculates an aperture height of 1 m. In the results shown here, the aperture heights approach 1 m at high impedances, and degrade as the impedance decreases, as we expect.

Next, we calculate the power-normalized gain, $h_a/f_g^{1/2}$, which one optimizes when a fixed amount of power is available (Figure 4.6). The peak for the two-arm case occurs at $Z_c = 412.6\ \Omega$, where $G_p = 0.7789$ m. The peak for the four-arm case occurs at $Z_c = 505.6\ \Omega$, where $G_{p4} = 0.7455$ m. Note that these values of gain are lower than the corresponding gains of the circular-cone feed in the previous section.

Finally, we calculate the voltage-normalized gain, h_a/f_g, which one optimizes when a fixed voltage level is available (Figure 4.7). The peak for the two-arm case occurs at $Z_c = 232.3\ \Omega$, where $G_p = 0.8727$ m. The peak for the four-arm case occurs at $Z_c = 371.3\ \Omega$, where $G_{p4} = 0.7004$ m. Note that adding a second pair of arms in this case introduces a significant penalty in performance.

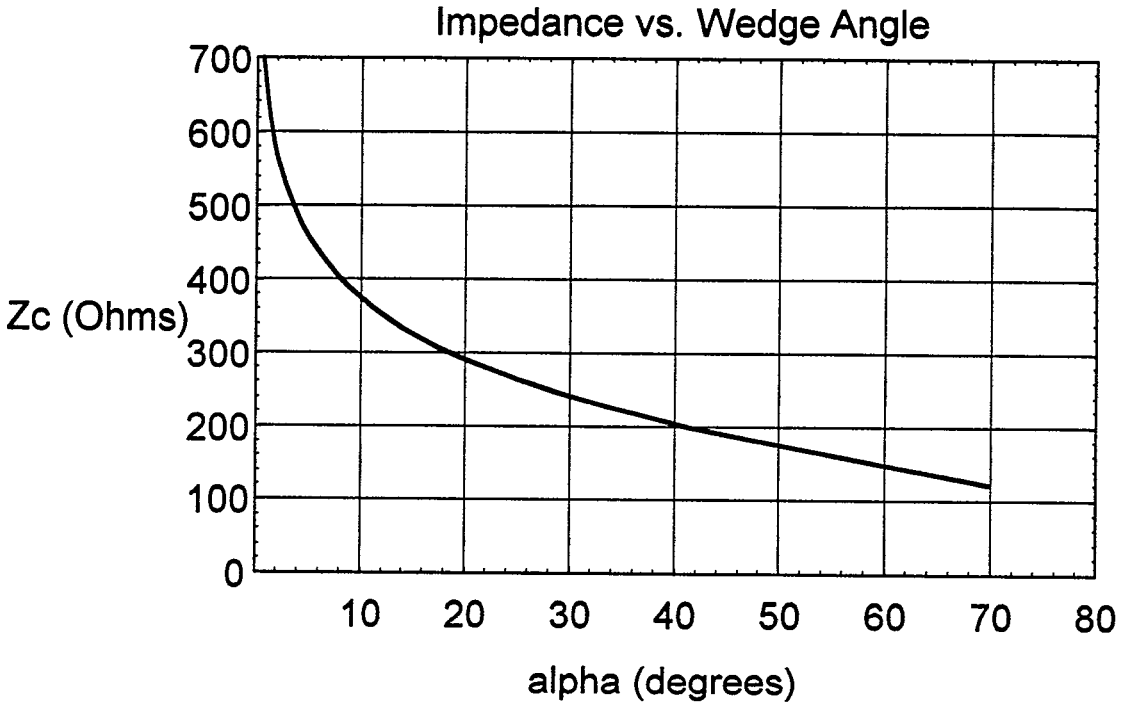

Figure 4.4. Characteristic impedance as a function of α for two curved plates.

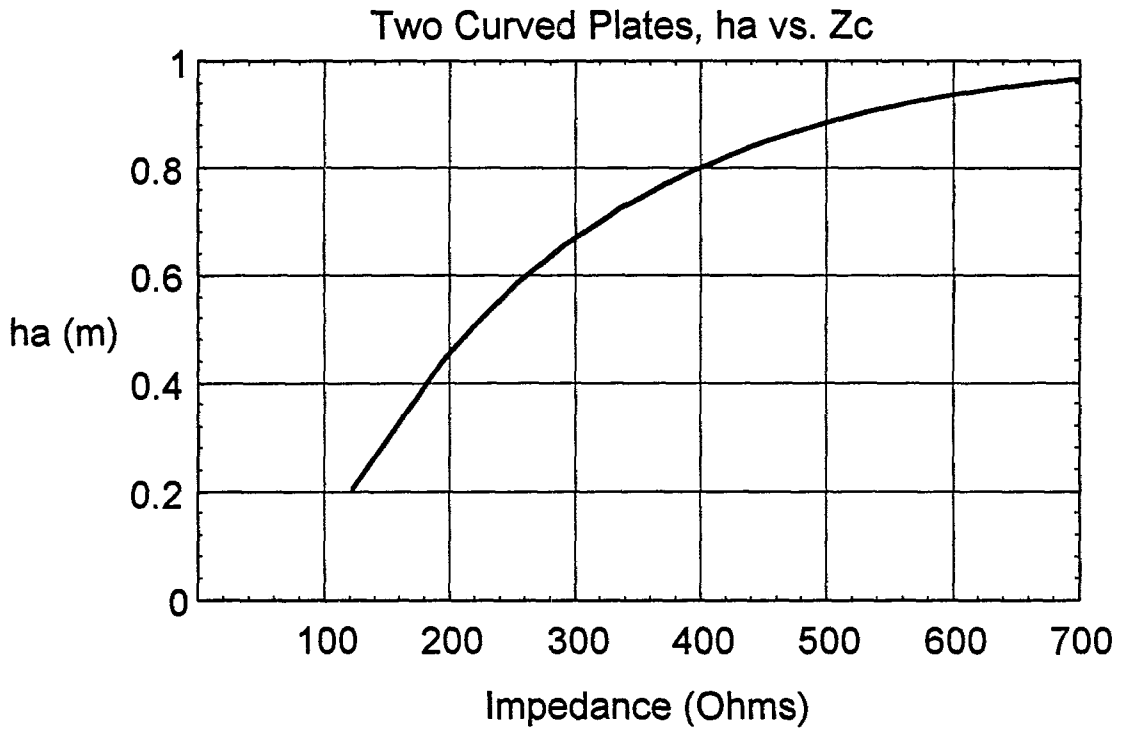

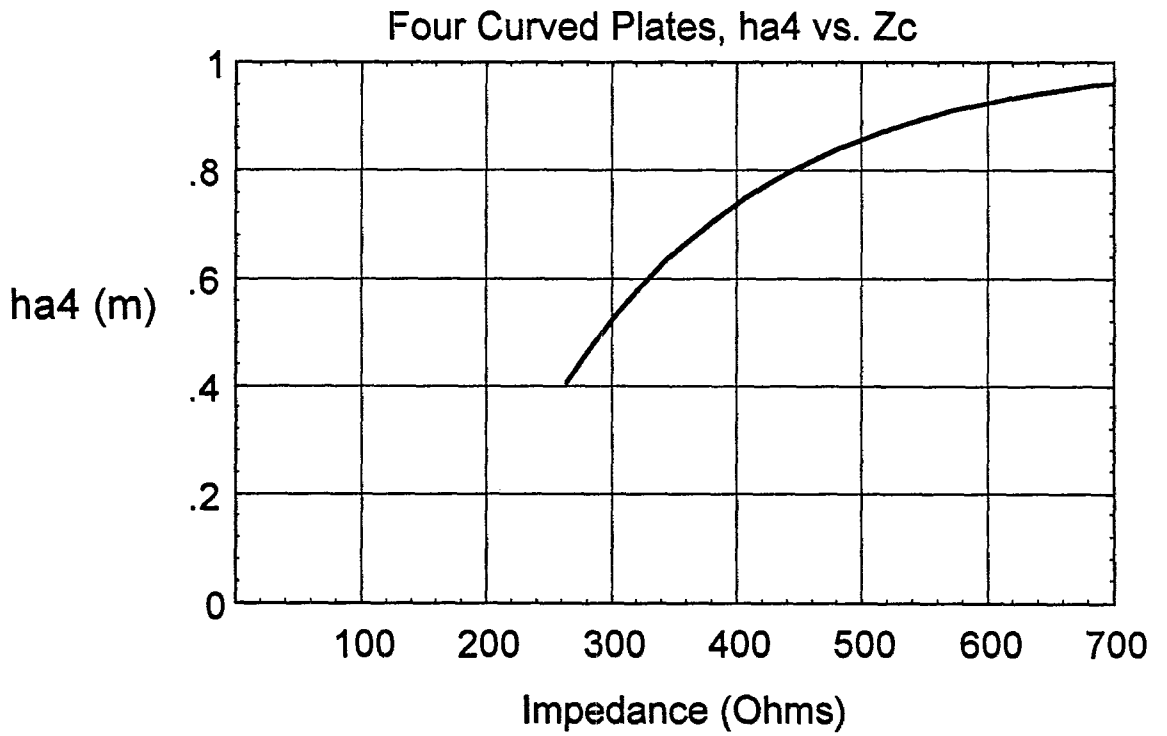

Figure 4.5. Aperture heights as a function of feed impedance for curved plates, two-arm (top) and four-arm (bottom) configurations.

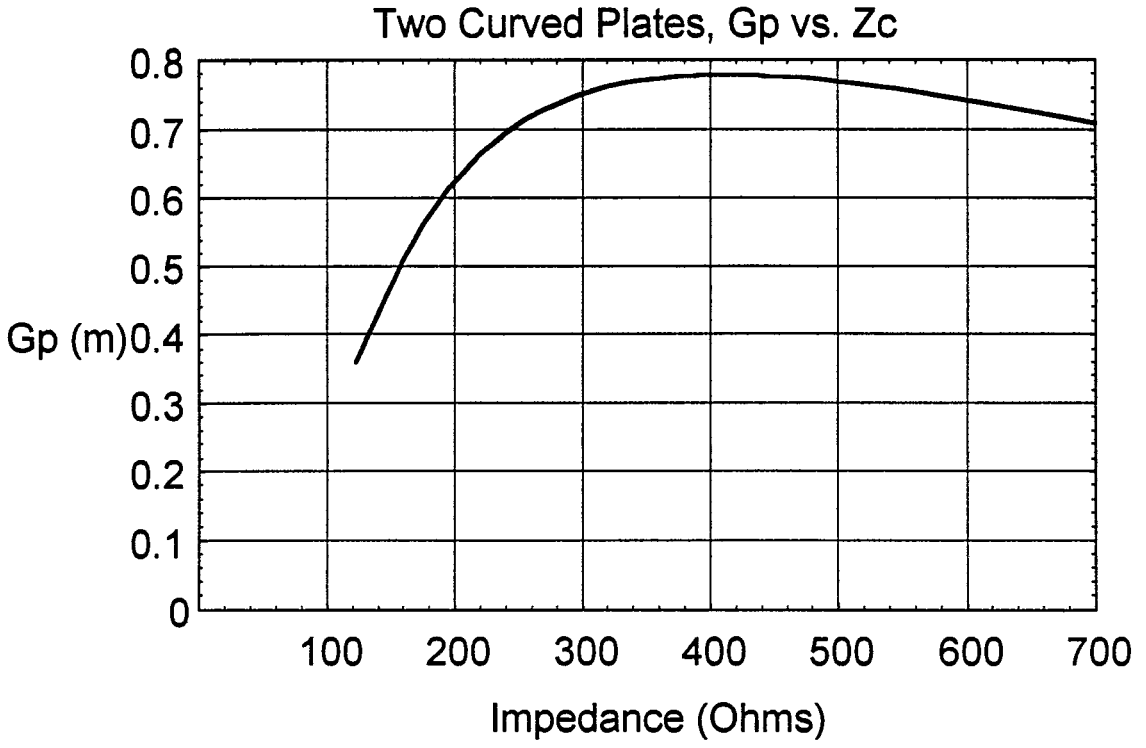

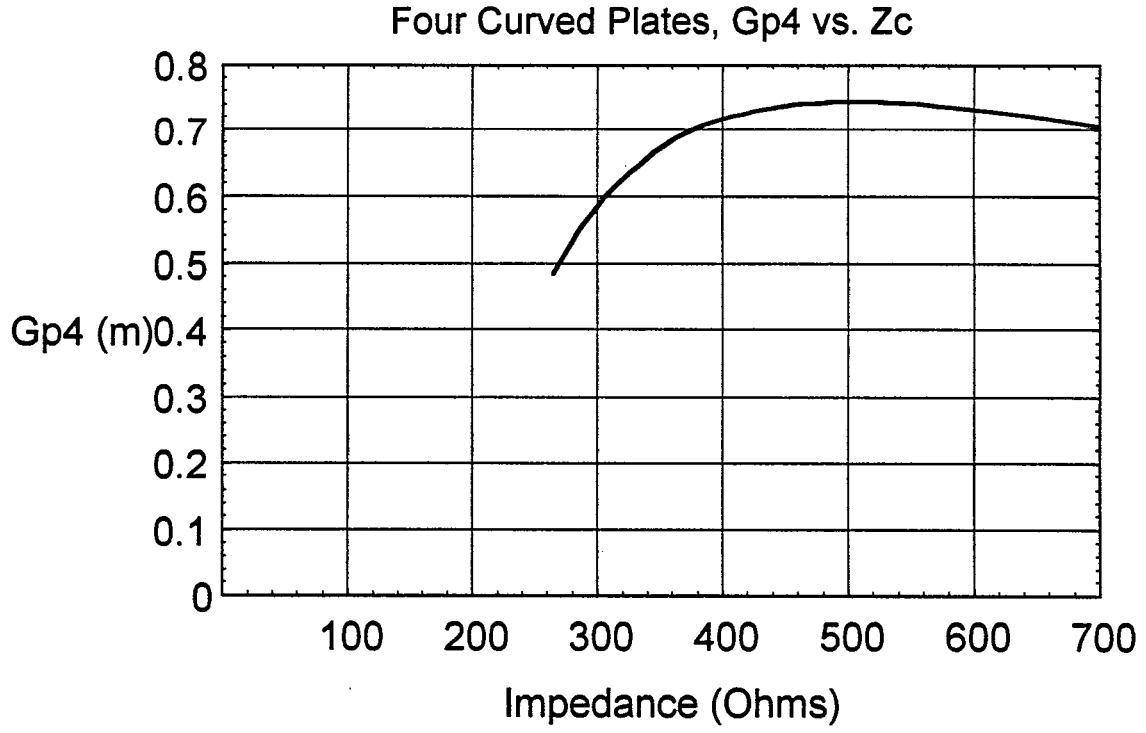

Figure 4.6. Power normalized gain as a function of feed impedance for curved plate feeds. The two-arm case (top) has a peak of $G_p = 0.7789$ m at $Z_c = 412.6\ \Omega$. The four-arm case (bottom) has a peak of $G_{p4} = 0.7455$ m at $Z_c = 505.6\ \Omega$.

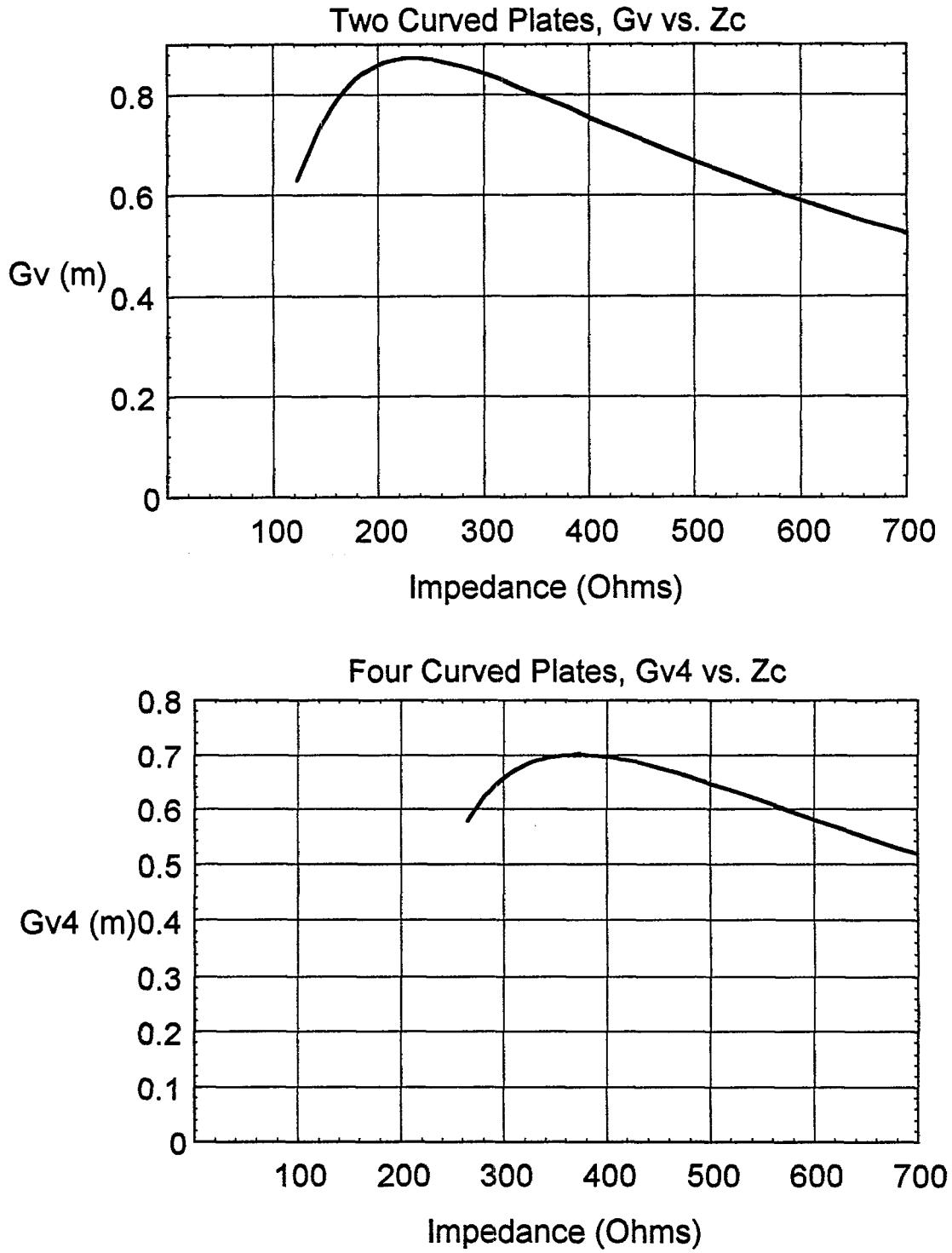

Figure 4.7. Voltage normalized gain as a function of feed impedance for curved plate feeds. The two-arm case (top) has a peak of $G_v = 0.8727$ m at $Z_c = 232.3\ \Omega$. The four-arm case (bottom) has a peak of $G_{v4} = 0.7004$ m at $Z_c = 371.3\ \Omega$.

V. Coplanar Plates

Finally, we consider the configuration of coplanar plates (Figure 5.1). This is an appealing configuration, since there is no aperture blockage, at least using our simple approximation of geometrical optics. Although there is no aperture blockage, the approximation that the aperture height is equal to the aperture radius breaks down at low impedances. The approximation is still very good at higher impedances. As usual, we work the problem for an aperture of radius 1 m.

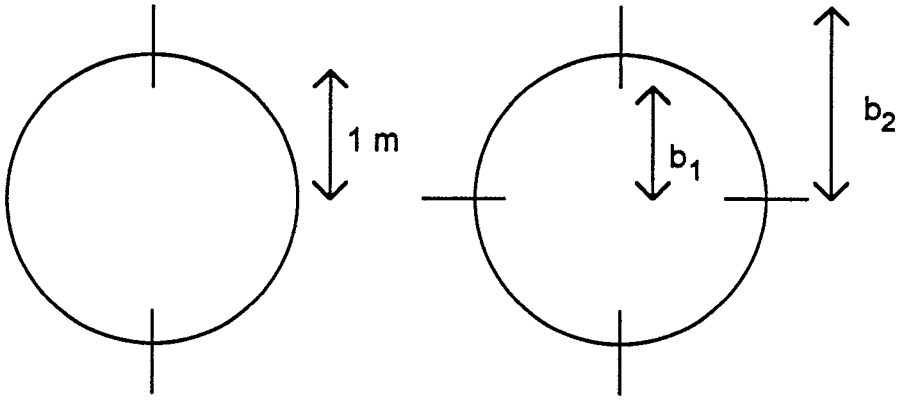

Figure 5.1. Projection of the coplanar plate configuration onto the aperture plane, 2-arm and 4-arm configurations.

The potential function for this configuration is adapted slightly from [11] as

$$w(z) = \operatorname{arcsn}\left(-jm^{-1/4}z\right), \qquad z = jm^{1/4}\operatorname{sn}(w) \tag{5.1}$$

where the arcsn function is the inverse of the Jacobian elliptic sn function, and

$$m = \frac{b_1^2}{b_2^2}, \qquad b_1 = m^{1/4}, \qquad b_2 = m^{-1/4} \tag{5.2}$$

Furthermore, the characteristic impedance is $Z_o f_g$, where

$$f_g = \frac{K(m)}{K(1-m)} = \frac{K(m)}{K'(m)} \tag{5.3}$$

An approximate potential function map is plotted in Figure 5.2.

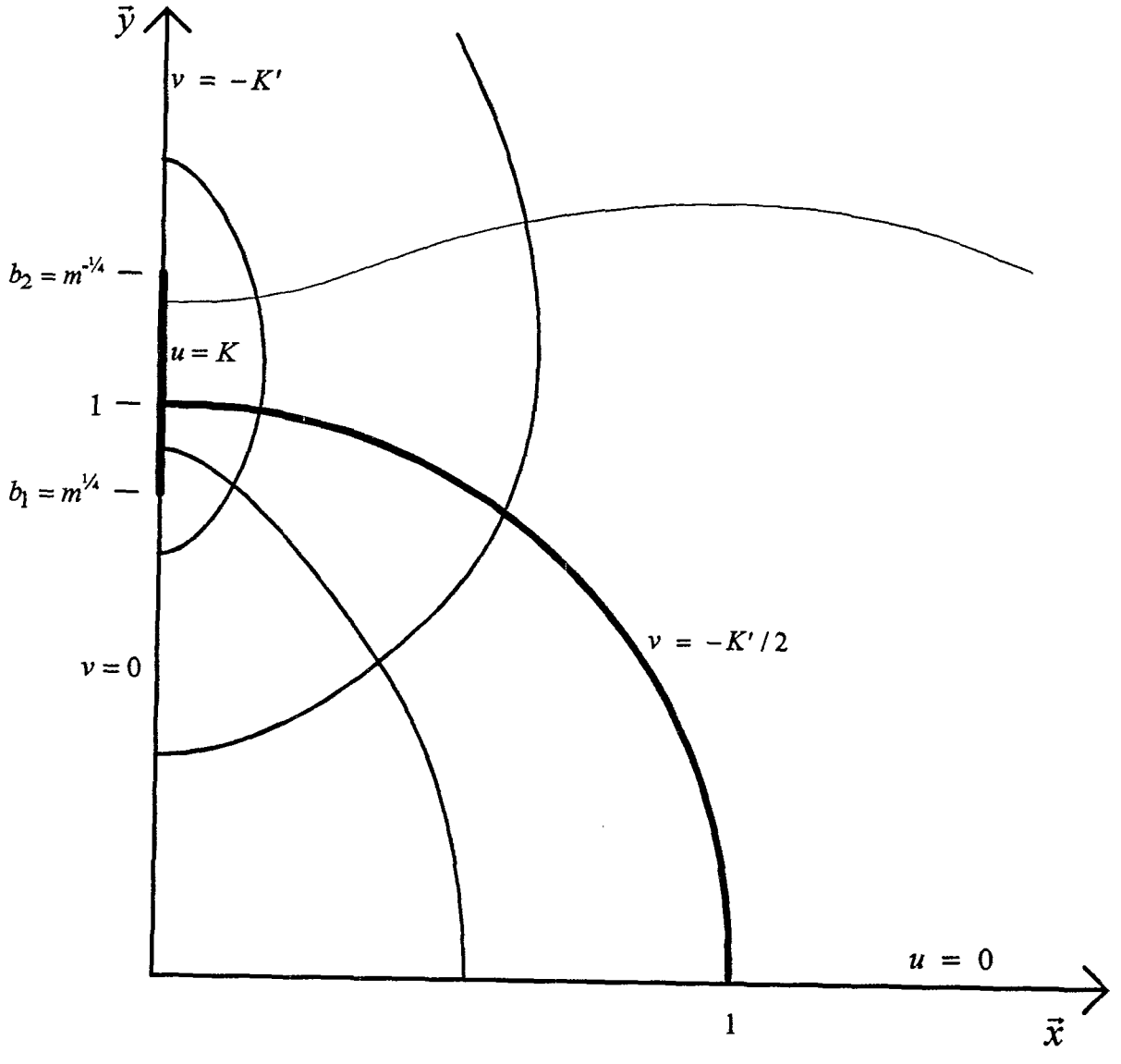

Figure 5.2. Approximate complex potential map for coplanar plates. A more accurate diagram of a closely related configuration appears in [11, p. 71].

As usual, we need to find the aperture height

$$h_a = -\frac{4}{\Delta v} \oint_{C_a'} v(y)\, dy \tag{5.4}$$

where Δv is the change in v around one of the conductors, in this case $2K'$. Interestingly, we need to calculate this only for the 2-arm case, since the integral for the four-arm case is identical. This is a true no matter how low the feed impedance is, since the second pair of arms does not affect the integral.

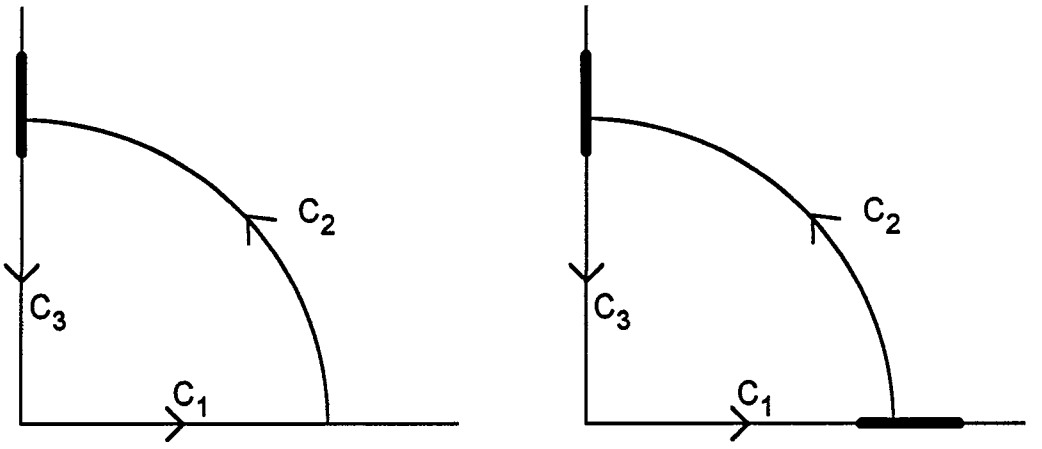

Figure 5.3. Contours for the coplanar plate aperture integration, 2-arm and 4-arm arrangements.

Before proceeding to the contour integral calculation, we need to prove that the contour C_2, described by $x^2+y^2=1$, also lies on the contour $v = -K'/2$. To demonstrate this, we note that [9, p. 575],

$$\mathrm{sn}(u+jv|m) = \frac{\mathrm{sn}(u|m)\,\mathrm{dn}(v|m_1) + j\,\mathrm{cn}(u|m)\,\mathrm{dn}(u|m)\,\mathrm{sn}(v|m_1)\,\mathrm{cn}(v|m_1)}{\mathrm{cn}^2(v|m_1) + m\,\mathrm{sn}^2(u|m)\,\mathrm{sn}^2(v|m_1)} \tag{5.5}$$

Substituting this into (5.1), and noting that $v = -K'/2$, we find

$$x = \frac{\mathrm{cn}(u|m)\,\mathrm{dn}(u|m)}{1+m^{1/2}\,\mathrm{sn}^2(u|m)}, \qquad y = \frac{\left(1+m^{1/2}\right)\mathrm{sn}(u|m)}{1+m^{1/2}\mathrm{sn}^2(u|m)} \tag{5.6}$$

on the contour C_2. Note also that [9, p. 573]

$$1-m-\mathrm{dn}^2(u|m) = -m\,\mathrm{cn}^2(u|m) = m\,\mathrm{sn}^2(u|m) - m \tag{5.7}$$

By combining (5.6) and (5.7) one can show with a little algebra that $x^2+y^2=1$ on the contour described by $v = -K'/2$.

Let us now calculate the contour integral. The contours to be followed are shown in Figure 5.3. Along C_1, $dy = 0$, so $I_1 = 0$. Along C_2, we have just proven that $v = -K'/2$, so

$$I_2 = \int_{C_2} v(y)\, dy = -\frac{K'(m)}{2} \tag{5.8}$$

Finally, along C_3, $v = 0$ for the portion of the curve not touching the feed arm, so there is no contribution. Where it touches, there is a contribution. Thus, $z = j\,y$ along C_3, so the integral is

$$I_3 = \int_{C_3} v(y)\, dy = \int_1^{m^{1/4}} \mathrm{Im}\left(\mathrm{arcsn}\left(m^{-1/4}\, y\right)\right) dy \tag{5.9}$$

It is simplest to evaluate the above integral numerically, by using a program such as Mathematica, which has the inverse sn function built in. However, it is possible to evaluate this function analytically, in closed form. One can obtain some interesting results by generating the closed form solution, so it is worth the extra effort.

We begin the evaluation of I_3 by noting that on the upper plate $u(z) = K$, so

$$w(y) = K + j\, v(y) = \mathrm{arcsn}\left(m^{-1/4} y\right) \tag{5.10}$$

It is straightforward to show that $\mathrm{sn}(K + j\,v \,|\, m) = \mathrm{nd}(v \,|\, m_1)$, so on the upper plate

$$v(y) = \mathrm{arcnd}\left(m^{-1/4} y \,|\, m_1\right) \tag{5.11}$$

where the nd function is one of the Jacobian elliptic functions, and arcnd is its inverse. This simplifies the evaluation of I_3 to

$$\begin{aligned} I_3 &= \int_1^{m^{1/4}} v(y)\, dy = \int_1^{m^{1/4}} \mathrm{arcnd}\left(m^{-1/4} y \,|\, m_1\right) dy \\ &= m^{1/4} \int_{m^{-1/4}}^{1} \mathrm{arcnd}(y' \,|\, m_1)\, dy' \end{aligned} \tag{5.12}$$

where $y' = m^{-1/4}\, y$. It is unclear how to carry out the above integration directly, however, one can differentiate the above integrand simply. This makes the integral a good candidate for integration by parts. Thus, the derivative is [13, p. 286]

$$\frac{d}{dy'}\operatorname{arcnd}(y'|m_1) = \frac{1}{\sqrt{(y'^2-1)(1-m\,y'^2)}} \tag{5.13}$$

Using this, the integral becomes

$$\begin{aligned} I_3 &= m^{1/4}y'\operatorname{arcnd}(y'|m_1)\Big|_{y'=m^{-1/4}}^{1} - m^{1/4}\int_{m^{-1/4}}^{1}\frac{y'\,dy'}{\sqrt{(y'^2-1)(1-m\,y'^2)}} \\ &= \frac{K'}{2} - m^{1/4}\int_{m^{-1/4}}^{1}\frac{y'\,dy'}{\sqrt{(y'^2-1)(1-m\,y'^2)}} \end{aligned} \tag{5.14}$$

If we now make the substitution $\xi = y'^2$, we have

$$\begin{aligned} I_3 &= \frac{K'}{2} - \frac{m^{1/4}}{2}\int_{m^{-1/2}}^{1}\frac{d\xi}{\sqrt{(\xi-1)(1-m\,\xi)}} \\ &= \frac{K'}{2} - \frac{m^{1/4}}{2}\int_{m^{-1/2}}^{1}\frac{d\xi}{\sqrt{-1+(m+1)\xi-m\,\xi^2}} \end{aligned} \tag{5.15}$$

The integral now simplifies by using [14, p.81]

$$\int\frac{dx}{\sqrt{a+bx+cx^2}} = \frac{-1}{\sqrt{-c}}\arcsin\left(\frac{2cx+b}{\sqrt{b^2-4ac}}\right) \tag{5.16}$$

which is valid for $c < 0$ and $4ac - b^2 < 0$. Thus we have

$$I_3 = \frac{K'}{2} - \frac{m^{-1/4}}{2}\left[\frac{\pi}{2} - \arcsin\left(\frac{(1-m^{1/2})^2}{m_1}\right)\right] \tag{5.17}$$

This completes the evaluation of I_3.

Finally, let us calculate h_a using (5.4). The total effective height is just

$$h_a = -\frac{2}{K'}(I_2 + I_3) \tag{5.18}$$

where I_2 is given in (5.8), and I_3 is given in (5.17). Thus, we have

$$h_a = \frac{\pi m^{-1/4}}{2K'}\left[1 - \frac{2}{\pi}\arcsin\left(\frac{(1-m^{1/2})^2}{m_1}\right)\right] \tag{5.19}$$

As we said earlier, this is valid for both the 2-arm and 4-arm configurations. The asymptotic limit of this expression at high impedances, for $m \to 1$ or $m_1 \to 0$, is

$$h_a \to 1 - \frac{m_1}{2\pi} = 1 - \frac{1}{2\pi}\left[1 - \frac{b_1^2}{b_2^2}\right] \tag{5.20}$$

which converges to the correct answer for high impedances. This concludes the evaluation of h_a.

We can make an interesting comparison now between the analytic form of h_a and some other results obtained for circular aperture distributions [15]. It was shown in [15] that for a circular aperture whose aperture field could be expressed as a sum of circular harmonics (i.e., a TEM field with no singularities internal to the aperture), and whose time dependence was a uniform step function, the radiated far field on boresight is

$$E(z,t) = \frac{E_o a^2}{2cr}\delta_a(t - r/c) \tag{5.21}$$

where a is the aperture radius, r is the distance out on boresight, and E_o is the field at the center of the aperture. Furthermore, the function $\delta_a(t)$ is the approximate delta function that has appeared in many earlier papers. For the current geometry of coplanar plates, the field at the center of the aperture is

$$E_o = \frac{V}{2Ka}\left.\frac{du(x=0,y)}{dy}\right|_{y=0} = \frac{V}{2Ka}\left.\frac{d}{dy}\operatorname{arcsn}(m^{-1/4}\,y)\right|_{y=0} = \frac{V m^{-1/4}}{2aK} \tag{5.22}$$

Thus, if the theory of [15] held true for the current geometry, we would expect a radiated field of

$$E(z,t) = \frac{V}{r}\frac{a m^{-1/4}}{4cK}\delta_a(t - r/c) \tag{5.23}$$

Comparing this to (2.4), we have an effective aperture height h_a of

$$h_a = \frac{\pi f_g a}{2K} = \frac{\pi a m^{-1/4}}{2K'} \tag{5.24}$$

This is clearly different from the effective height developed in (5.19), which we know must be correct. In fact, it is exactly the first term of (5.19). (Recall that (5.19) was calculated based on an aperture radius of unity, so we must multiply the result of (5.19) by the radius a in order to

make a direct comparison.) We therefore conclude that the theory of [15] does not hold in this case, perhaps because of the presence of the metal in the aperture, which gives a singularity in the aperture fields. It is worthwhile to note, however, that the expression in (5.24) approaches the aperture radius a at high impedances, as it must. Thus, the two expressions are equivalent in the limit as $b_1/b_2 \rightarrow 1$.

Let us now present our results. First, we show a plot of Z_c as a function of b_1/b_2, and as a function of b_1 (Figure 5.4). We do so since all subsequent results are provided in terms of the feed impedance.

Next, we plot the aperture height as a function of Z_c in Figure 5.5. At high impedances there is relatively little degradation, however as one approaches zero impedance the effective height does tend toward zero. This is not due to aperture blockage; this simply represents a more accurate calculation that what was done previously. Recall that we expect an aperture height of 1 m only as an approximation at high impedances [3]. This calculation is valid for both two-arm and four-arm configurations.

The power-normalized gain, $h_a/f_g^{1/2}$, is shown in Figure 5.6. For this configuration we get a peak of 0.9132 m at an impedance of 301.8 Ω. Note that this peak occurs at about the same impedance as with the circular cone feed (311.9 Ω), however, the peak power-normalized gain for that case was only 0.8491 m. Thus, we do see the effects of aperture blockage. Even more interesting is to compare the four-arm cases. The same peak of 0.9132 m is still valid for the co-planar plate case. But for the circular cones the peak power-normalized gain is only 0.8060 m. Thus, the improvement with coplanar plates becomes even more significant with four arms.

Finally, we plot the voltage-normalized gain, h_a/f_g, in Figure 5.7. For this case, the peak occurs at zero Ohms, so one is limited by the amount of the feed arm one can allow to project beyond the edge of the reflector.

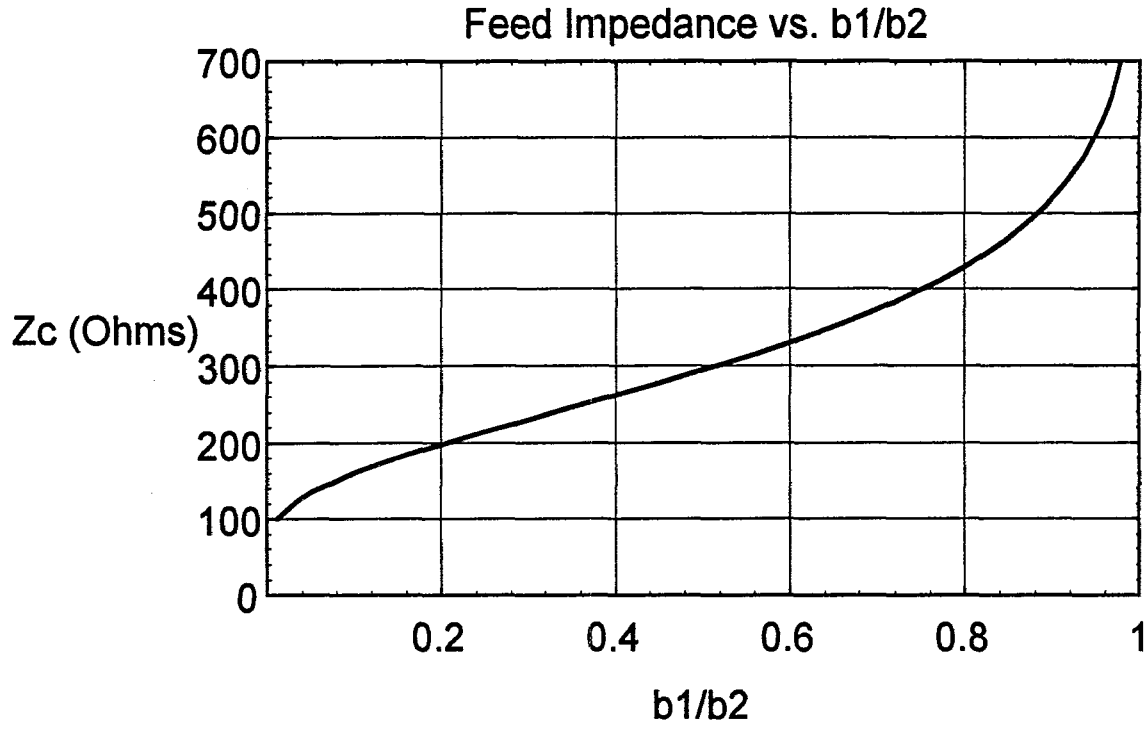

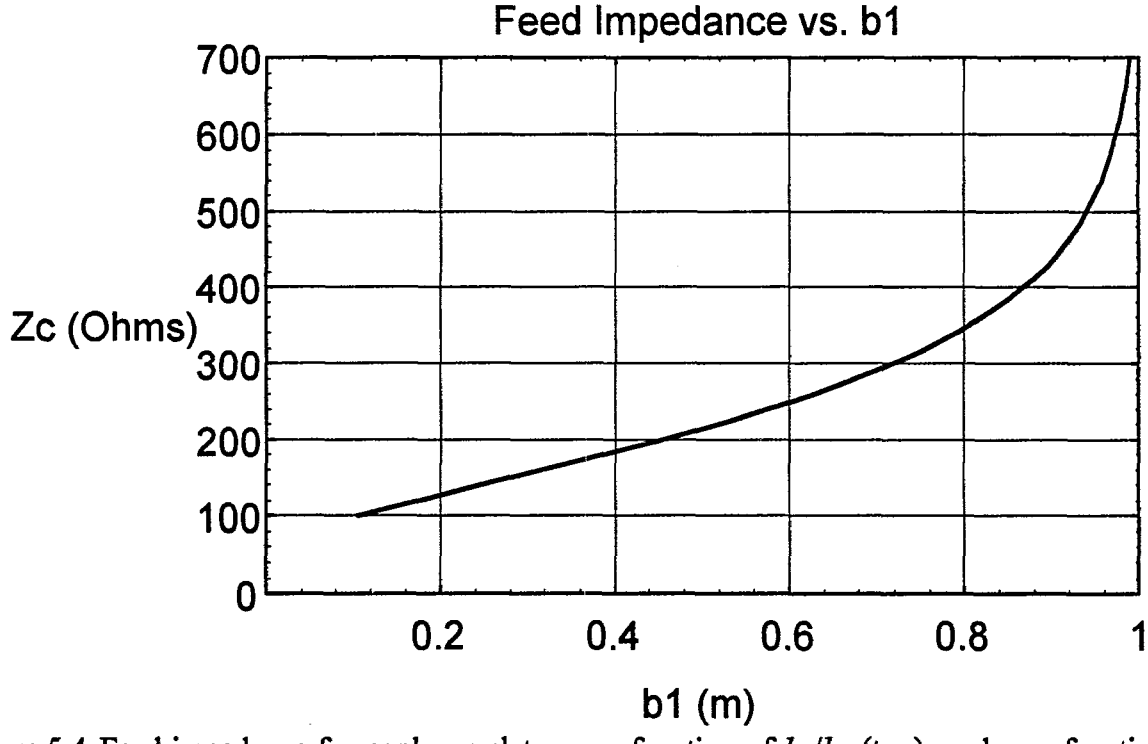

Figure 5.4. Feed impedance for coplanar plates as a function of b_1/b_2 (top), and as a function of b_1 (bottom) for a radius of 1 m.

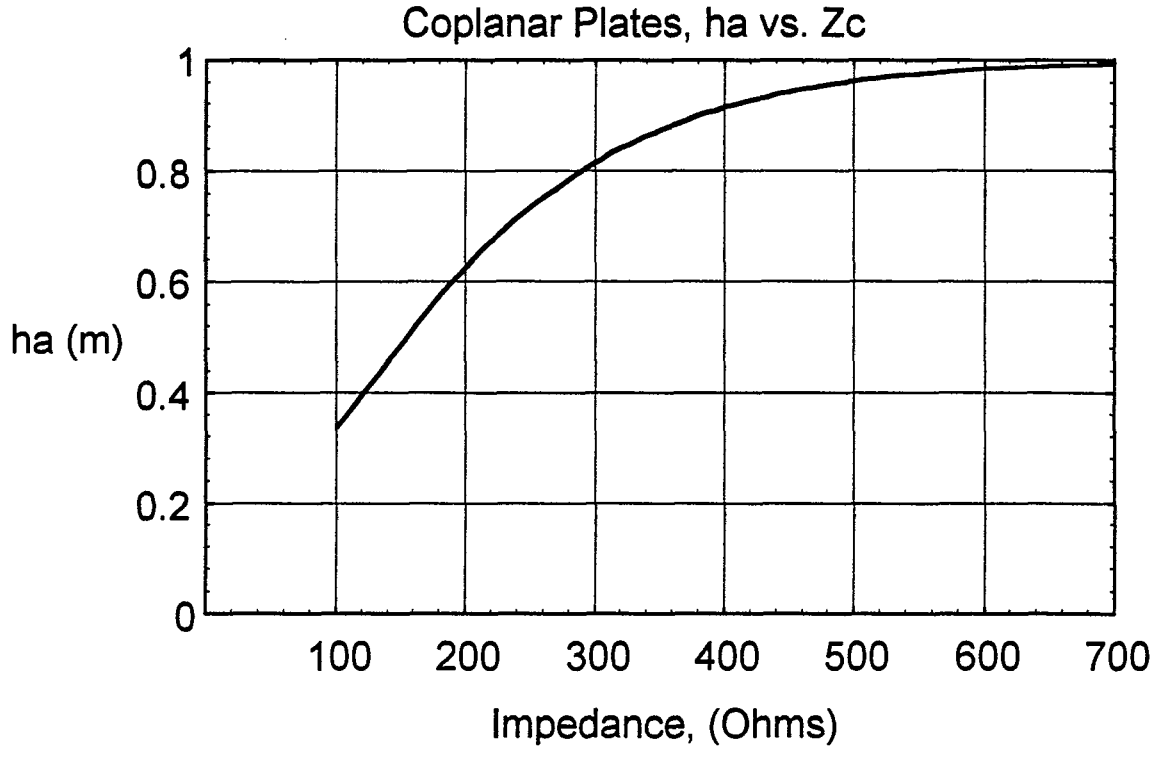

Figure 5.5. Aperture height as a function of feed impedance for coplanar plate feeds.

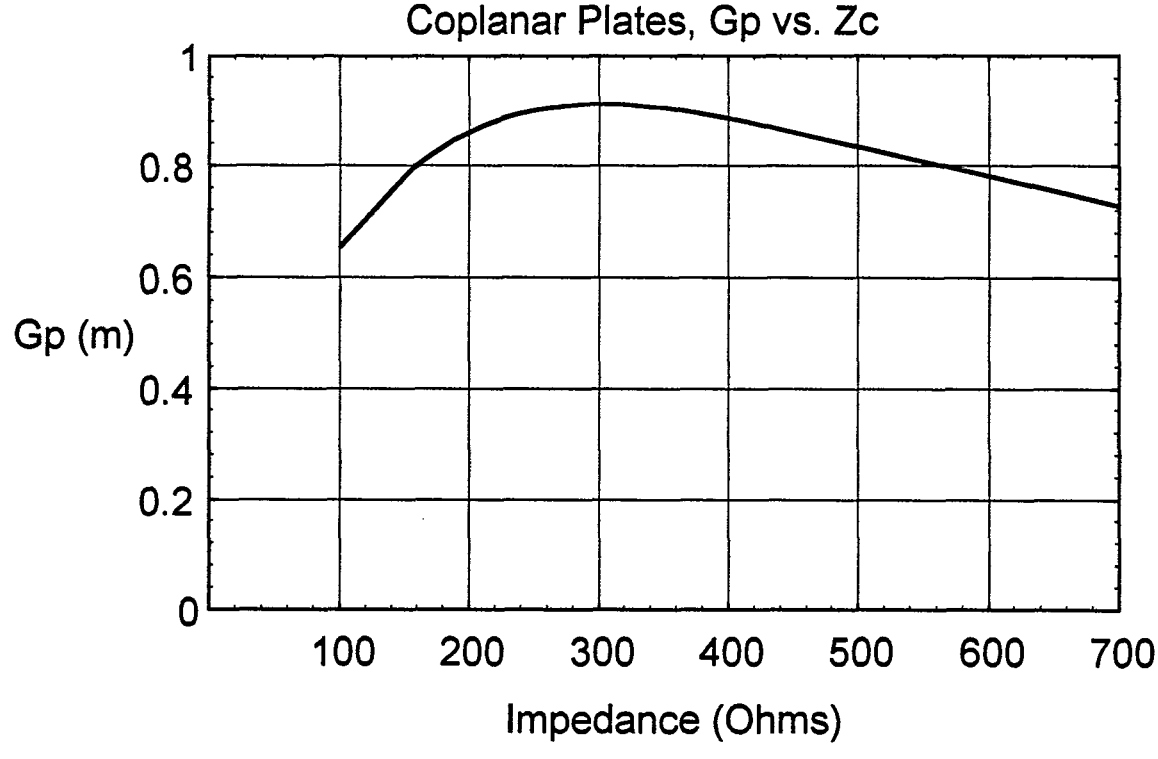

Figure 5.6. Power normalized gain as a function of feed impedance for coplanar plate feeds. The peak is $h_a = 0.9132$ m at $Z_c = 301.8\ \Omega$.

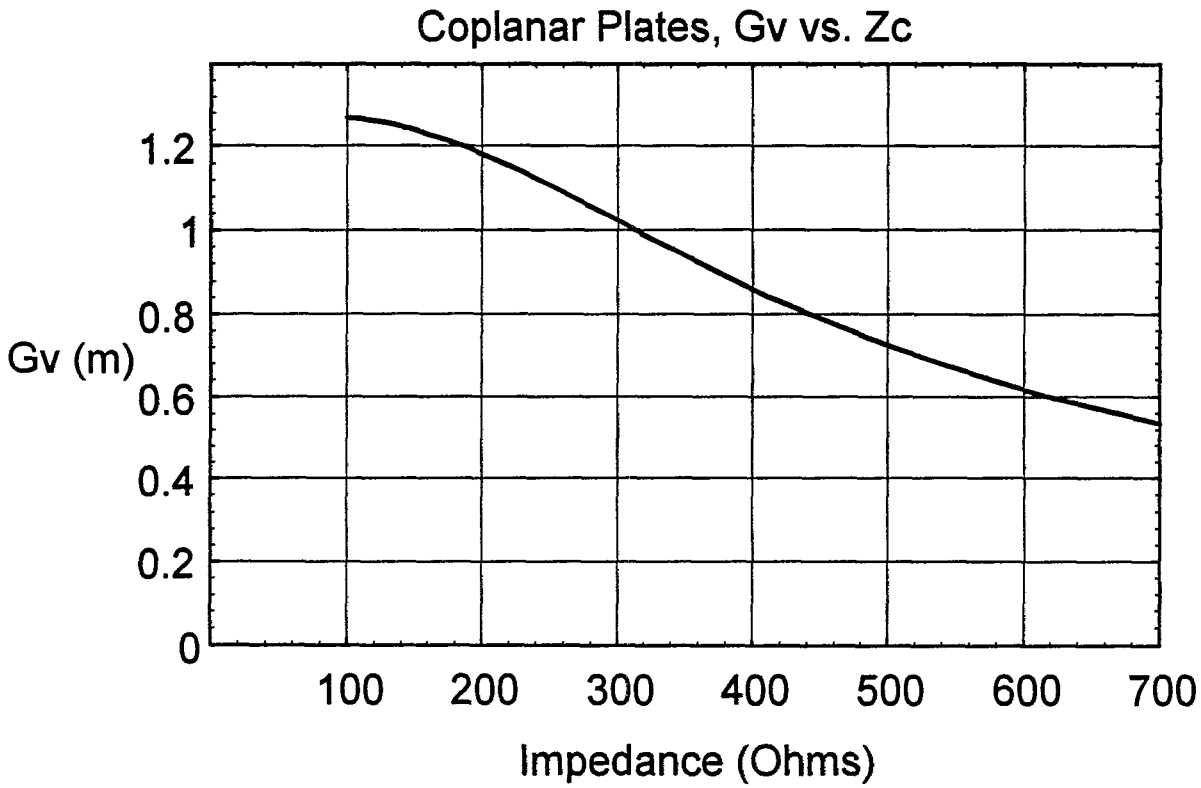

Figure 5.7. Voltage-normalized gain as a function of feed impedance for coplanar plate feeds.

VI. Discussion

For most of the configurations discussed here, there are maxima in the gains that optimize the radiated field. It should be pointed out, however, that these peaks tend to be rather broad, so one can miss the optimal feed impedance by a fair amount, and still be within ten percent or so of the maximum gain.

One question that remains is whether or not a second pair of arms increases the radiated field. Consider first the case of constant input power. With two arms, one feeds the antenna with a voltage V. With four arms, one connects pairs of arms in parallel, thereby rotating the field by 45° [10]. Now each pair of opposite arms is fed with half the power, or a voltage of $V/2^{1/2}$, assuming the same impedance for each pair of arms as for the two-arm case. Since the maximum field is polarized at an angle of 45° to either pair of arms, there is no net effect if one ignores feed blockage. If one includes feed blockage there is a slight disadvantage with using four arms. The total radiated field with four arms is down by a factor of h_{a4}/h_a from the two-arm case. Since this ratio is equal to one for the coplanar plate case, in this case there is no penalty at all. On the other hand, there is a significant advantage in using four arms, since doing so reduces the input impedance by a factor of two. This could be important when matching the antenna impedance to the source impedance, since source impedances are typically lower than antenna impedances. Another use of the second pair of arms is that it allows one to transmit two polarizations.

Next, consider the case of constant voltage. The constraint we used was that the voltage across each pair of opposite arms was set to some maximum, which was determined by the breakdown properties of the medium. This constraint makes sense for the two-arm configuration, but it requires some modification in order to make sense in the four-arm configuration. In a two-arm configuration the maximum voltage across the two arms is V. In a four-arm configuration, if voltage breakdown occurs, it occurs between oppositely charged arms that are next to each other, rather than opposite to each other. This, in practice, would limit the total sustainable voltage between two opposite arms to be somewhat less than V. If it were $V/2^{1/2}$, then once again the second pair of arms would introduce a small penalty in the radiated field, quantified as h_{a4}/h_a. However, in general this arrangement should be able to sustain somewhat more than $V/2^{1/2}$. In fact, for thin wires, it is known that four wires can sustain a voltage of almost V. Thus, the second pair of feed arms might allow an increase in the radiated field by somewhat less than $2^{1/2}$ of the total radiated field, depending on the details of the feed structure. Clearly more work will be needed to clarify the four-arm case when limited by voltage breakdown.

Certain feed impedances are natural choices. For example, a feed impedance that is 50 Ω times an even integer exponent of 2 ($50\ \Omega \times 2^{2N}$) is convenient when building a balun or impedance transformer (with turns ratio $1{:}N$). For this reason, a feed impedance value of 400 Ω for two feed arms (effectively 200 Ω with four feed arms) was previously thought to represent a good tradeoff between low feed impedance and minimal aperture blockage. The results generated here tend to confirm that the maximum occurs in the vicinity of 400 Ω for most of the sets of constraints in which we might be interested. If the optimum radiated field is required, however, we now understand how to choose the feed impedance. This might be useful, for example, if no balun were required, or if one fed the antenna with an impedance other than 50 Ω.

VII. Conclusion

In this paper we have described a simple technique for trading off low feed impedances in an IRA against aperture blockage. The technique involved a contour integration that included more terms than earlier works had calculated, thereby accounting for aperture blockage. Optimizations were carried out based on constraints of constant input power and constant input voltage. Configurations with both two arms and four arms were analyzed. A later paper will provide similar results for a long TEM horn, or a TEM horn with a lens in the aperture (lens IRA).

Acknowledgment

We wish to thank Dr. Carl E. Baum for many helpful discussions on this subject. We also wish to thank Phillips Laboratory for funding this work.

References

1. E. G. Farr and C. E. Baum, Prepulse Associated with the TEM Feed of an Impulse Radiating Antenna, Sensor and Simulation Note 337, March 1992.

2. E. G. Farr, Simple Models of Antennas Useful in Ultra-Wideband Applications, Transient Radiating Antenna Memo 2, July 1992.

3. C. E. Baum, Aperture Efficiencies for IRAs, Sensor and Simulation Note 328, June 24, 1991.

4. Y. Rahmat-Samii, Analysis of Blockage Effects on TEM-Fed Paraboloidal Reflector Antennas, Sensor and Simulation Note 347, October 25, 1992.

5. Y. Rahmat-Samii and D. V. Giri, Analysis of Blockage Effects on TEM-Fed Paraboloidal Reflector Antennas (Part II: TEM Horn Illumination), Sensor and Simulation Note 349, November 3, 1992.

6. E. G. Farr and C. E. Baum, Extending the Definitions of Antenna Gain and Radiation Pattern Into the Time Domain, Sensor and Simulation Note 350, November 1992.

7. C. E. Baum, Impedances and Field Distributions for Symmetrical Two Wire and Four Wire Transmission Line Simulators, Sensor and Simulation Note 27, October 10, 1966.

8. T. K. Liu, Impedances and Field Distributions of Curved Parallel-Plate Transmission-Line Simulators, Sensor and Simulation Note 170, February 1973.

9. M. Abramowitz and I. Stegun, *Handbook of Mathematical Functions*, National Bureau of Standards, Applied Mathematics Series 55, December 1972.

10. C. E. Baum, Configurations of TEM Feed for an IRA, Sensor and Simulation Note 327, April 27, 1991.

11. P. Moon and D. E. Spencer, *Field Theory Handbook*, Springer Verlag, 1971.

12. Wolfram Research, Inc., *Mathematica, A System for Doing Mathematics by Computer*, version 2.1, July 1992.

13. P. F. Byrd and M. D. Friedman, *Handbook of Elliptic Integrals for Engineers and Scientists*, Second Edition, Springer-Verlag, 1971.

14. I. S. Gradshteyn and I. M. Ryzhik, *Tables of Integrals, Series, and Products*, Academic Press, 1980.

15. C. E. Baum, Circular Aperture Antennas in Time Domain, Sensor and Simulation Note 351, November 2, 1992.